Unified Stochastic Geometry Modeling and Analysis of Cellular Networks in LOS/NLOS and Shadowed Fading

Imène Trigui, *Member, IEEE*, Sofiène Affes, *Senior Member, IEEE*, and Ben Liang, *Senior Member, IEEE*

***Abstract*— Statistical characterization of the signal-to-interference-plus-noise ratio (SINR) via its cumulative distribution function is ubiquitous in a vast majority of technical contributions in the area of cellular networks, since it boils down to averaging the Laplace transform of the aggregate interference, a benefit accorded at the expense of confinement to the simplistic Rayleigh fading. In this paper, to capture diverse fading channels that arise in realistic outdoor/indoor wireless communication scenarios, we tackle the problem differently. By exploiting the moment generating function of the SINR, we succeed in analytically assessing cellular networks performance over the shadowed κ–μ, κ–μ, and η–μ fading models. These channel models offer high flexibility by capturing diverse fading channels, including Rayleigh, Nakagami-*m*, Rician, and Rician shadow fading distributions. These channel models have been recently promoted for their capability to accurately model dense urban environments, future femtocells, and device-to-device shadowed channels. In addition to unifying the analysis for different channel models, this paper integrates the coverage, the achievable rate, and the bit error probability, which are largely treated separately in the literature. The developed model and analysis are validated over a broad range of simulation setups and parameters.**

***Index Terms*— 5G, cellular networks, moment generating function, line-of-sight (LoS), non-line-of-sight (NLoS), shadowing, stochastic geometry.**

I. Introduction

CELLULAR networks modeling and analysis is a vibrant topic that keeps taking new dimensions in complexity as to mirror the evolution if not revolution of wireless networks from the first to the upcoming fifth wireless technology generation (5G). As a key enabler to realize 5G wireless networks, heterogeneous networks (HetNets) are indeed the most influential solution that guarantees higher data rates and macrocell traffic off-loading, while providing dedicated capacity to homes, enterprises, or urban hot spots. To cope with such evolution, stochastic geometry proved to be a very powerful tool for reproducing large-scale spatial randomness, an intrinsic property of emerging cellular networks, as well as different sources of uncertainties (such as multipath fading, shadowing, and power control) within tractable and accurate mathematical frameworks [1], [3]. Able to provide insightful design guidelines, through closed forms, stochastic geometry rid system-level performance evaluation of computationally-intensive simulations.

In the last decade, many contributions spearheaded this line of research by developing all aspects of the stochastic geometry models, except for the fading environments. For instance, the downlink baseline operation of cellular networks is characterized in [1]–[5]. Range expansion and load balancing are studied in [6] and [7]. By exploiting recent advances in stochastic geometry analysis, several mathematical frameworks are developed to study multiple-input multiple output (MIMO) operation in cellular networks [8], [9]. Other aspects including energy efficiency, energy harvesting, interference cancellation, additional interference imposed via underlay device-to-device (D2D) communication, etc., have been investigated exploiting the tractability of stochastic geometry (see [10] and references therein).

As far as the fading model is concerned, the Rayleigh fading has been commonly assumed, with only some proposals incorporating the Nakagami-*m* fading, yet merely with integer parameter values [5], [11]. Such particular fading distributions, by leading to exponential expressions for the conditional SINR that enable averaging via the MGF of the interference, have very often implied very similar mathematical models in their analysis steps. Strikingly, due to the Rayleigh assumption, characterizing the SINR via its cumulative distribution function (CDF) is ubiquitous in almost all pioneering contributions pertaining to cellular networks modeling [1]–[10].

Such infatuation with Rayleigh and Nakagami-*m* has, however, limited legitimacy according to [12] and [13], who argued that these fading models may fail to capture new and more realistic fading environments. Besides ignoring the line-of-sight (LOS) component in the received signal, which is prominent in outdoor cellular communications, the Rayleigh model is a single-parameter fading model that is not flexible enough to accurately represent complex indoor fading environments. The diagnosis for Rayleigh fading is even more pessimistic in future femtocells [14] where multiple dominant signal components (DSCs) may be created by reflections in close proximity to the BSs and/or users or may appear in millimeter wave (mmW) communications [15]. With Nakagami-*m* fading, stochastic geometry analysis necessitates for tractability an

Manuscript received September 26, 2016; revised February 19, 2017 and May 29, 2017; accepted July 3, 2017. Date of publication July 27, 2017; date of current version December 15, 2017. The associate editor coordinating the review of this paper and approving it for publication was M. Di Renzo. *(Corresponding author: Imène Trigui.)*

I. Trigui and B. Liang are with the University of Toronto, Toronto, ON M5S 3G4, Canada (e-mail: imene.trigui@ece.utoronto.ca).

S. Affes is with INRS, Montreal, QC H5A 1K6, Canada.

Color versions of one or more of the figures in this paper are available online at http://ieeexplore.ieee.org.

Digital Object Identifier 10.1109/TCOMM.2017.2732444

integer value for m [11], thereby limiting the applicability of the model in setup scenarios that capture practical multipath conditions. Despite the fact that several approaches show alternative techniques to circumvent such dependency to the Rayleigh fading [16]–[19]; there are yet no stochastic geometry models accounting for state-of-the-art fading models

As a step forward to bridge this gap in the literature, this work incorporates versatile multiple-parameter fading models into tractable stochastic geometry analysis. These fading models include the shadowed κ-μ distribution, the generalized Rician or the κ-μ distribution, and the η-μ distribution. Besides their elegance, these models are governed by more than two tunable parameters endowing them with high flexibility to capture a broad range of fading channels, whence their practical significance. The κ-μ distribution, first introduced in [12], can be regarded as a generalization of the classic Rician fading model for line-of-sight (LOS) scenarios. On the other hand, the η-μ distribution can be considered as a generalization of the classic Nakagami-q (Hoyt) fading model for non-LOS scenarios. Interestingly, the κ-μ and the η-μ distributions represent all-encompassing generalizations, with the classical channels including the Nakagami-m, the Hoyt, the Rayleigh, and the Rice fading being their special cases.

The shadowed κ-μ fading model, recently introduced in [20], jointly includes large-scale and small-scale propagation effects, by considering that only the dominant components are affected by shadowing [20]. The shadowed κ-μ distribution includes the shadowed Rician distribution as a special case, and obviously it also includes the κ-μ fading distribution from which it originates. However, as we will later see, one of the most appealing properties of the shadowed κ-μ distribution is that it unifies the set of LOS fading models associated with the κ-μ distribution [12], and strikingly, it also unifies the set of NLOS fading models associated with the η-μ distribution [12]. These fading models offer far better and much more flexible representations of practical fading LOS, NLOS, and shadowed channels than the Rayleigh and Nakagami-m distributions.

Although some works have considered already shadowed κ-μ fading in the context of stochastic geometry [21], [22], they relied on series representation methods (e.g., infinite series in [21] and Laguerre polynomial series in [22]) thereby expressing the interference functionals as an infinite series of higher order derivative terms given by the Laplace transform of the interference power. These methods cannot lend themselves to closed-form expressions and hence require complex numerical evaluation.

To the best of the authors' knowledge, this paper is pioneer in introducing a general approach of incorporating the comprehensive shadowed κ-μ, κ-μ and η-μ fading models into an exact and unified stochastic geometry analysis. Besides offering a unified modeling framework for the analysis of a much wider set of practical fading distributions, this work also develops a unified mathematical analysis paradigm for three key performance metrics altogether: i) the average BEP, ii) the coverage probability, and iii) the ergodic achievable rate for cellular networks.

The rest of the paper is organized as follows. The system model, assumptions, and methodology of our new analysis framework are presented in Section II. In Section III, the baseline downlink modeling paradigm for cellular networks over LOS/NLOS and shadowed fading is presented. Our new unified performance analysis framework is presented in section IV. Numerical and simulation results are presented in Section V and the paper is concluded in Section VI.

II. Network and Channel Models

We consider a downlink single-tier cellular network where single-antennas BSs are deployed according to a homogeneous PPP Ψ with intensity λ and a typical single-antenna mobile user is located at the origin. It is assumed that all the BSs have the same transmit power P. Without loss of generality, all BSs are assumed to have an open access policy, and hence, all users can associate with all BSs. The users are assumed to associate to the BSs according to their average radio signal strength (RSS). Similar to [1], universal frequency reuse is considered with no intra-cell interference.

Further, we adopt the standard path-loss propagation model of power attenuation $r^{-\alpha}$ with the propagation distance r, where $\alpha > 2$ is the path-loss exponent. For simplicity, we assume that all BSs experience the same path-loss exponent α. Besides we assume that the channel gains between any two generic locations, denoted by h, include all random channel effects such as fading and shadowing. Additionally, we assume the latter to be independent of each other, independent of the spatial locations, symmetric, and identically distributed. We introduce below some key definitions for the generic channel model distributions adopted in this work.

A. Channel Model Distributions

Definition 1 (The Shadowed κ-μ Distribution [20]): Let h be a random variable statistically following a shadowed κ-μ distribution with mean $\Omega = \mathcal{E}[h]$ and non-negative real shape parameters κ, μ, and m, i.e., $h \sim S_{\kappa,\mu,m}(\Omega; \kappa, \mu, m)$. Then its probability density function (PDF) is given by

$$f_{h,S\kappa-\mu}(y) = \frac{\mu^{\mu} m^{m} (1+\kappa)^{\mu}}{\Gamma(\mu)\Omega^{\mu}(\mu\kappa+m)^{m}} \left(\frac{y}{\Omega}\right)^{\mu-1} e^{-\frac{\mu(1+\kappa)}{\Omega}y} \times {}_1\mathrm{F}_1\left(m, \nu, \frac{\mu^2\kappa(1+\kappa)}{\Omega(\mu\kappa+m)}y\right), \quad (1)$$

where ${}_1\mathrm{F}_1(\cdot)$ is the confluent hypergeometric function of [23, eq. (13.1.2)] and the Gamma function is denoted by $\Gamma(\cdot)$ [23]. The shadowed κ-μ fading model was originally proposed in [20]. In recent works, the shadowed κ-μ distribution provided an excellent fit with channel measurements conducted to characterize the shadowed fading observed in device-to-device communication channels [24] and in shadowed body-centric communication channels [25]. In this new model, the potential clustering of multipath components is considered alongside the presence of elective dominant signal components (DSCs), which are subject to Nakagami-m distribution. The shadowed κ-μ distribution is an extremely versatile fading model that also includes as special cases other important distributions such as the One-Sided Gaussian, Rice, Nakagami-m, and Rayleigh distributions.

Definition 2 (The κ-μ Distribution [12]): Let h be a random variable statistically following a κ-μ distribution with mean

$\Omega = \mathcal{E}[h]$ and non-negative real shape parameters κ and μ, i.e., $h \sim S_{\kappa,\mu}(\Omega; \kappa, \mu)$. Then its pdf is given by

$$f_{h,\kappa-\mu}(y) = \frac{\mu(1+\kappa)^{\frac{\mu+1}{2}}}{e^{\kappa\mu}\Omega\kappa^{\frac{\mu-1}{2}}} \left(\frac{y}{\Omega}\right)^{\frac{\mu-1}{2}} e^{-\frac{\mu(1+\kappa)}{\Omega}y} \times \mathrm{I}_{\mu-1}\left(2\mu\sqrt{\frac{\kappa(1+\kappa)}{\Omega}y}\right), \quad (2)$$

where the modified Bessel function of the first kind of order b is represented by $\mathrm{I}_b(\cdot)$ [23, eq. (8.431.1)]. The κ-μ fading model was originally conceived for modeling the small-scale variations of a fading signal under LOS conditions in non-homogeneous environments. If $\mu = 1$, this distribution reduces to the Rice model. The latter is the most important model for representing a single dominant DSC between the BS and a mobile user [26]. However, multiple DSCs may be created by reflections from metal objects (e.g., light-posts, cars) in close proximity to the BSs and/or users, or may appear in millimeter wave (mmW) communications where highly directional antennas are used for short-range communications [15]. Therefore, the κ-μ distribution offers a much more flexible representation of practical fading LOS channels than the Ricean one [13]. The κ-μ distribution is reduced from the shadowed κ-μ distribution by eliminating the shadowing of each dominant component when $m \longrightarrow \infty$.

Definition 3 (The η-μ Distribution [12]): Let h a random variable statistically following an η-μ distribution with mean $\Omega = \mathcal{E}[h]$ and non-negative real shape parameters η and μ, i.e., $h \sim S_{\eta,\mu}(\Omega; \eta, \mu)$. Then its pdf is given by

$$f_{h,\eta-\mu}(y) = \frac{\sqrt{\pi}(1+\eta)^{\mu+\frac{1}{2}}\mu^{\mu+\frac{1}{2}}}{\Gamma(\mu)\Omega\sqrt{\eta}(1-\eta)^{\mu-\frac{1}{2}}} \left(\frac{y}{\Omega}\right)^{\mu-\frac{1}{2}} e^{-\frac{\mu(1+\eta)^2}{2\eta\Omega}y} \times \mathrm{I}_{\mu-\frac{1}{2}}\left(\frac{\mu(1-\eta)^2}{2\eta\Omega}y\right). \quad (3)$$

Since it is practically difficult to achieve a LOS communication all the time, we consider, in this work, the η-μ distribution as a general fading distribution that can be used to better represent the small-scale variation of the fading signal in a NLOS condition [12]. If $\mu = m$ and $\eta \longrightarrow \infty$, this distribution reduces to the Nakagami-m model. Moreover, when $\mu = 1/2$, we obtain the Nakagami-q Hoyt distribution.

B. Modeling Methodology

The instantaneous SINR for the tagged user placed at the origin[1] and located at a random distance r from its serving BS can be expressed as

$$\mathrm{SINR} = \frac{Phr^{-\alpha}}{\sigma^2 + P\sum_{i\in\Psi^{(\backslash 0)}} h_i r_i^{-\alpha}} = \frac{hr^{-\alpha}}{\frac{\sigma^2}{P} + I}, \quad (4)$$

where σ^2 is the noise power, $\Phi^{(\backslash 0)}$ is the point process representing the interfering BSs (excluding the serving BS) on the tagged channel, and the random variable $I = \sum_{i\in\Psi^{(\backslash 0)}} h_i r_i^{-\alpha}$ denotes the aggregate interference at the tagged user from $\Psi^{(\backslash 0)}$. According to the properties of homogeneous PPPs [27, Vol. 1, Th. 1.4.5], the set of interfering BSs $\in \Phi^{(\backslash 0)}$ is still a homogeneous PPP outside the ball centered at the origin and of radius r. Note that in stochastic geometry analysis, spatial average performance metrics requires the pdf of r, which is given in a PPP network with RSS association as $f_r(x) = 2\pi\lambda x e^{-\pi\lambda x^2}, r \geq 0$ [1].

Lemma 1: The MGF of the SINR can be calculated as

$$M_{\mathrm{SINR}}(s) = 1 - 2\sqrt{s}\int_0^\infty \underbrace{\mathcal{E}_h\left[\sqrt{h}\mathrm{J}_1\left(2\sqrt{sh}\xi\right)\right]}_{\Sigma} \times \mathcal{E}_r\left[\exp\left(-\frac{\sigma^2}{P}\xi^2 r^\alpha\right)\mathcal{L}_I(\xi^2 r^\alpha)\right]d\xi, \quad (5)$$

where $\mathcal{E}_x[.]$ is the expectation with respect to the random variable x, $\mathrm{J}_1(\cdot)$ is the Bessel function of the first kind and first order [23, eq. (8.402)], and $\mathcal{L}_I(s) = \mathcal{E}\left[e^{-sI}\right]$ denotes the Laplace transform of the aggregate interference.

Proof: See Appendix A.

It is worth emphasizing that Σ in (5) is independent of the variable $\mathcal{L}_I$ and is a function of the fading parameters only. Hence, for known fading parameters, Σ is a constant w.r.t. the interference Laplace transform. This key property of Lemma 1 makes the latter a powerful baseline model to build upon in terms of developing tractable analytical models for cellular network, namely by extending the results of this paper to many other directions. Without any pretention of being able to discuss them all due to lack of space, the most prominent directions for future works include MIMO and multi-tier downlink performance analysis. Although extended in numerous ways to date [1]–[10], these models (i.e., downlink and multi-tier) have never been considered from the standpoint of (5). Interestingly, Lemma 1 not only promotes general and generic fading channels, but also other generalization aspects such as the the effect of LOS/NLOS propagation where the probability with which a BS is NLOS (also termed blocking probability) is dependent on the distance between the BS and the receiver of interest [28]. In this context, leveraging on Lemma 1, mathematical models for millimeter wave (mmWave) cellular communications, regarded as a potential scheme in next fifth generation (5G) systems and Internet of things (IoT) applications, become tractable. Remarkably, the proposed framework is also able to accommodate both closest- and strongest-BS association rules as well as single- and multi-slope path loss models [29].

Hereafter, by applying (5), we characterize the SINR by deriving its MGF in generalized fading channels. In contrast to almost all existing works that adopt the CCDF-based analysis approach [1]–[11] owing to the tractability and favorable analytical characteristics of Rayleigh fading, we develop a novel modeling paradigm for cellular networks that incorporates much more flexible and useful fading models, namely shadowed κ-μ, κ-μ, and η-μ into a novel tractable stochastic geometry analysis framework. Capitalizing on the several existing MGF-based approaches for performance analysis namely the Gil-Pelaez inversion theorem [30] for coverage probability, the transforms for rate analysis of Hamdi [31] and Di Renzo *et al.* [32], Craig's transform for BEP analy-

[1] Based on the properties of homogeneous PPPs, there is no loss of generality in assuming the tagged user to be located at the origin [27].

sis [26], and fractional moment calculation for error vector magnitude (EVM) performance [33], this work develops a unified mathematical paradigm that bridges the gap between BEP, coverage probability, and ergodic rate analyses in cellular networks. Extension of this analysis framework to cover performance metrics (EVM, average throughput,[2] etc.) under the considered generic fading models is beyond the scope of this contribution and will be the subject of future works.

III. Unified Analysis of the SINR Statistics

We now state our main and most general results from which all other results in the subsequent sections shall follow.

Theorem 1: The MGF of the SINR over shadowed κ-μ fading is

$$M_{\mathrm{SINR}}^{S\kappa\mu}(s) = 1 - \frac{\Omega s}{\left(\frac{\mu\kappa}{m}+1\right)^m (1+\kappa)} \int_0^\infty \Psi_1 \times\left(\mu+1, m; 2, \mu; \frac{-s\xi\Omega}{\mu(1+\kappa)}, \frac{\mu\kappa}{\mu\kappa+m}\right)\mathcal{E}_r \times\left[\exp\left(-\xi r^\alpha \frac{\sigma^2}{P}\right)\mathcal{L}_I^{S\kappa\mu}\left(\xi r^\alpha\right)\right] d\xi, \quad (6)$$

where $\Psi_1(\cdot,\cdot;\cdot,\cdot;\cdot,\cdot)$ denotes the Humbert function of the first kind [34, eq. (1.2)], and $\mathcal{L}_I^{S\kappa\mu}$ denotes the Laplace transform of the aggregate interference when the receiver interfering link suffers from shadowed κ-μ fading, i.e., $h_{i\in\Phi^{(\backslash 0)}} \sim S_{\kappa,\mu,m}(\Omega_I;\kappa_I,\mu_I,m_I)$, with integer valued m_I and μ_I, obtained as

$$\mathcal{L}_I^{S\kappa\mu}(\xi r^\alpha) = \exp\Bigg(-2\pi\lambda r^2\Bigg(\sum_{k=1}^{m_I}\frac{\binom{k}{m_I}\Xi^k\xi^k}{\alpha k-2}\,{}_2\mathrm{F}_1 \times\left(m_I, k-\frac{2}{\alpha}, k+1-\frac{2}{\alpha}, -\Xi\xi\right) - \sum_{n=1}^{m_I-\mu_I}\frac{\binom{n}{m_I-\mu_I}\Theta^n\xi^n}{\alpha n-2}\,{}_2\mathrm{F}_1 \times\left(m_I, n-\frac{2}{\alpha}, n+1-\frac{2}{\alpha}, -\Xi\xi\right)\Bigg)\Bigg), \quad (7)$$

when $\mu_I \le m_I$. And when $\mu_I \ge m_I$, it becomes

$$\mathcal{L}_I^{S\kappa\mu}(\xi r^\alpha) = \exp\Bigg(-2\pi\lambda r^2 \sum_{n,k;(n,k)\neq(0,0)}^{m_I,\mu_I-m_I}\frac{\binom{\mu_I-m_I}{k}\binom{m_I}{n}\Theta^k\Xi^n\xi^{k+n}}{\alpha(n+k)-2} \times \mathrm{F}_1\left(n+k-\frac{2}{\alpha}, \mu_I-m_I, m_I, n+k+1-\frac{2}{\alpha}, -\Theta\xi, -\Xi\xi\right)\Bigg), \quad (8)$$

where $\Theta = \frac{\Omega_I}{\mu_I(1+\kappa_I)}$, $\Xi = \frac{(\mu_I\kappa+m_I)\Omega_I}{m_I\mu_I(1+\kappa_I)}$. Moreover, ${}_2\mathrm{F}_1(a,b,c,x)$ and $\mathrm{F}_1(a,b,b';c;x,y)$ denote the Gauss hypergeometric function [23, eq. (9.100)] and the first Appell's hypergeometric function [23, eq. (9.180.1)], respectively, and $\binom{a}{b} = \Gamma(a)\Gamma(b)/\Gamma(a+b)$ is the binomial coefficient.

[2]Throughput is defined as the number of successfully transmitted bits per channel use.

Proof: See Appendix B.

Theorem 2: The MGF of the SINR over κ-μ fading is

$$M_{\mathrm{SINR}}^{\kappa\mu}(s) = 1 - \frac{\Omega e^{-\kappa\mu}s}{(1+\kappa)}\int_0^\infty \Psi_2\left(\mu+1; 2, \mu; \frac{-s\xi\Omega}{\mu(1+\kappa)}, \mu\kappa\right) \times \mathcal{E}_r\left[\exp\left(-\xi r^\alpha\frac{\sigma^2}{P}\right)\mathcal{L}_I^{\kappa\mu}\left(\xi r^\alpha\right)\right] d\xi, \quad (9)$$

where $\Psi_2(\cdot,\cdot;\cdot;\cdot,\cdot)$ denotes the Humbert function of the second kind [34, eq. (1.3)], and $\mathcal{L}_I^{\kappa\mu}$ denotes the Laplace transform of the aggregate interference under κ-μ fading, i.e., $h_{i\in\Phi^{(\backslash 0)}} \sim S_{\kappa,\mu}(\Omega_I;\kappa_I,\mu_I)$. Furthermore, when μ_I is integer $\mathcal{L}_I^{\kappa\mu}$ is obtained as

$$\mathcal{L}_I^{\kappa\mu}(\xi r^\alpha) = \exp\Bigg(-2\pi\lambda r^2\frac{\mu_I(1+\kappa_I)^{\mu_I}}{e^{\kappa_I\mu_I}\Omega_I^{\mu_I}}\sum_{k=0}^{\infty}\frac{\left(\frac{\mu_I^2\kappa_I(1+\kappa_I)}{\Omega_I}\right)^k}{k!} \times\sum_{n=1}^{\mu_I+k}\frac{\binom{\mu_I+k}{n}\,{}_2\mathrm{F}_1\left(\mu_I+k-2, n-\frac{2}{\alpha}, n+1-\frac{2}{\alpha}, \frac{-\xi\Omega_I}{\mu_I\kappa_I(1+\kappa_I)}\right)}{\left(\frac{\xi\Omega_I}{\mu_I\kappa_I(1+\kappa_I)}\right)^{-n}(\alpha n-2)}\Bigg). \quad (10)$$

Proof: See Appendix C.

Theorem 3: The MGF of the SINR over η-μ fading is

$$M_{\mathrm{SINR}}^{\eta\mu}(s) = 1 - \frac{2\Omega\eta^{\mu+1}s}{\eta+1}\int_0^\infty \Psi_1 \times\left(2\mu+1, \mu; 2, 2\mu; \frac{-s\xi\Omega\eta}{\mu(1+\eta)}, 1-\eta\right)\mathcal{E}_r \times\left[\exp\left(-\xi r^\alpha\frac{\sigma^2}{P}\right)\mathcal{L}_I^{\eta\mu}\left(\xi r^\alpha\right)\right] d\xi, \quad (11)$$

where the Laplace transform of the aggregate interference $h_{i\in\Phi^{(\backslash 0)}} \sim S_{\eta,\mu}(\Omega_I;\eta_I,\mu_I)$, denoted as $\mathcal{L}_I^{\eta\mu}$, is obtained as

$$\mathcal{L}_I^{\eta\mu}(\xi r^\alpha) = \exp\Bigg(-2\pi\lambda r^2\sum_{n,k;(n,k)\neq(0,0)}^{\mu_I,\mu_I}\frac{\binom{\mu_I}{k}\binom{\mu_I}{n}\eta_I^{-k}\left(\frac{\Omega_I\eta_I\xi}{\mu_I(1+\eta_I)}\right)^{n+k}}{\alpha(n+k)-2}\mathrm{F}_1 \times\left(n+k-\frac{2}{\alpha}, \mu_I, \mu_I, n+k+1-\frac{2}{\alpha}, \frac{-\Omega_I\xi}{\mu_I(1+\eta_I)}, \frac{-\Omega_I\eta_I\xi}{\mu_I(1+\eta_I)}\right)\Bigg). \quad (12)$$

Proof: From (1), when $m = \mu/2$, we resort to the reduction formula of ${}_1\mathrm{F}_1(\cdot)$ given by [23, eq. (9.6.47)]

$${}_1\mathrm{F}_1(\beta, 2\beta, z) = 2^{2\beta-1}\Gamma\left(\beta+\frac{1}{2}\right)z^{\frac{1}{2}-\beta}e^{z/2}\mathrm{I}_{\beta-\frac{1}{2}}\left(\frac{z}{2}\right), \quad (13)$$

readily yielding (3) after some algebraic manipulations. Previously shown in [35], this result reveals that the η-μ fading distribution arises as a particular case of the more general shadowed κ-μ model. Notice that, the Nakagami-q (Hoyt) model with shape parameter $q = \frac{1}{\sqrt{2\kappa+1}}$ arises when $m = \frac{\mu}{2} = 0.5$, since $\eta = q^2$ for the η-μ distribution in (3) [35].[3] Accordingly, the SINR MGF under η-μ fading is obtained

[3]The η-μ fading model is symmetrical for $\eta \in [0,1]$ and $\eta \in [1,\infty]$.

from (6) by setting $\underline{m} = \mu$, $\underline{\mu} = 2\mu$, and $\underline{\kappa} = \frac{1-\eta}{2\eta}$. Since $m_I = \mu_I/2 \leq \mu_I$, then $\mathcal{L}_I^{\kappa\mu}$ reduces from $\mathcal{L}_I^{S\kappa\mu}$ in (8) by setting $\underline{m}_I = \mu_I$, $\underline{\mu}_I = 2\mu_I$, and $\underline{\kappa}_I = \frac{1-\eta_I}{2\eta_I}$, thereby yielding (12).

Corollary 1: The MGF of the SINR over arbitrary Nakagami-m fading is given by

$$M_{\text{SINR}}^{m}(s) = 1 - \Omega s \int_0^{\infty} {}_1\text{F}_1\left(m+1, 2; \frac{-s\Omega\xi}{m}\right) \times \mathcal{E}_r\left[\exp\left(-\frac{\xi r^{\alpha}\sigma^2}{P}\right)\mathcal{L}_I^{m}\left(\xi r^{\alpha}\right)\right] d\xi, \quad (14)$$

and the Laplace transform of the aggregate interference under Nakagami-m $\mathcal{L}_I^m$ is given by

$$\mathcal{L}_I^{m}(\xi r^{\alpha}) = \exp\left(-\pi\lambda r^2\left({}_2\text{F}_1\left(-\frac{2}{\alpha}, m_I, 1-\frac{2}{\alpha}; -\frac{\Omega_I}{m_I}\xi\right)-1\right)\right). \quad (15)$$

Proof: The Nakagami-m fading distribution arises as a particular case of the more general shadowed κ-μ model when $m = \mu$. However, this simplification is not straightforward and actually requires further involved manipulations given in Appendix D.

It is worthwhile to note that $\mathcal{L}_I^m$ in (15) is a well-known result in the area of cellular networks analysis over Nakagami-m fading [9], [11]. While $\mathcal{L}_I^m$ has so far been presented as a fundamental finding in previous works, it becomes in this contribution a secondary result that simply reduces from a more general performance analysis framework.

The MGF of the SINR for Rayleigh fading, extensively adopted in the literature [1]–[10], reduces simply from (14) when $m = m_I = 1$ as

$$M_{\text{SINR}}(s) = 1 - \Omega s \int_0^{\infty} \exp(-s\Omega\xi)\mathcal{E}_r \times \left[\exp\left(\frac{-\xi r^{\alpha}\sigma^2}{P}\right)\mathcal{L}_I\left(\xi r^{\alpha}\right)\right] d\xi, \quad (16)$$

where the Laplace transform of the aggregate interference under Rayleigh fading, $\mathcal{L}_I$, is a special case of (15) when $m_I = 1$.

Proof: This proof is a special case of *Theorem 4* with more simplifications arising from the fact that ${}_1\text{F}_1(a, a; x) = \exp(x)$.

For completeness, it is worthwhile to mention that (16) can be easily deduced from CCDF-based analysis frameworks [1]–[10] by applying $M(s) = 1 - s\mathcal{L}_{\mathbb{P}(\text{SINR}>T)}(s)$ where $\mathbb{P}(\text{SINR} > T)$ is the CCDF of the SINR, given for instance in [1] as $\mathbb{P}(\text{SINR} > T) = \mathcal{E}_r\left[\exp(-\frac{T}{P\Omega}r^{\alpha}\sigma^2)\mathcal{L}_I\left(\frac{T}{\Omega}r^{\alpha}\right)\right]$, and carrying the change of variable $\xi = T/\Omega$. This key observation, unambiguously, corroborates the much wider scope claimed by our novel analysis framework and the rigor of its mathematical derivations.

While applying the shadowed κ-μ or the κ-μ (to capture different DSCs scenarios) to the tagged user link is quite intuitive (typically in the case of future femtocells and picocells), it might not be as much obvious to do so to the interference links. Actually, in a typical urban deployment, interfering channels are less likely to experience LOS than the direct link. However, destructive LOS interference may also happen in practice, namely in suburban and rural areas having wide parks and open spaces. In this work, the treatment of the tagged user link is independent from its interference counterpart as can be seen from (5). This dissociation is very appreciable since it allows modeling cellular networks with direct and interfering links experiencing asymmetric fading (i.e., different fading models). Although not shown explicitly in this work, cellular networks performance under asymmetric fading can be easily assessed by swapping $\mathcal{L}_I$ in (7), (8), (10), (12), and (15).

The new fundamental statistics disclosed in Theorems 1 to 4 provide a novel unifying analysis framework for of a variety of extremely important fading distributions. In some particular cases, the obtained formulas reduce to previously well-known major results in the literature. Besides, even though this work focuses on the shadowed κ-μ, κ-μ, and η-μ distributions, our new analysis framework is extensible to any other fading/shadowing distribution as long as the quantity pertaining to the expectation over h in (5) (i.e., Σ) can be obtained in closed form. Moreover, by assuming composite fading/shadowing fading over the interfering links, the analytical tractability of our new analysis framework is not affected at all and we can still formulate all performance metrics with the Laplace transform of the aggregate interference. Nevertheless, the expression of the latter might may become more involved.

IV. Average Achievable Rate

The average transmission rate, as defined by Shannon's capacity, is evaluated using the MGF transform in [31, Lemma 21] as

$$C \triangleq \mathcal{E}[\ln(1+\text{SINR})] = \int_0^{\infty} \frac{\exp\{-s\}}{s}\left(1 - M_{\text{SINR}}(s)\right) ds. \quad (17)$$

The average rate is computed in nats/Hz (1 bit = ln(2) = 0.6934 nats) for a typical user assumed to achieve the Shannon bound at its instantaneous SINR. We state now the main theorems that give the ergodic capacity of a typical mobile user on the downlink.

Theorem 5: The average ergodic rate of a typical mobile user on the downlink over shadowed κ-μ fading is

$$C^{S\kappa\mu}(\lambda, \alpha) = \frac{\Omega}{\left(\frac{\mu\kappa}{m}+1\right)^m(1+\kappa)}\int_0^{\infty} \text{F}_2 \times \left(\mu+1, m, 1; 2, \mu; \frac{\mu\kappa}{\mu\kappa+m}, \frac{-\xi\Omega}{\mu(1+\kappa)}\right)\mathcal{E}_r \times \left[\exp\left(-\xi r^{\alpha}\frac{\sigma^2}{P}\right)\mathcal{L}_I^{S\kappa\mu}\left(\xi r^{\alpha}\right)\right] d\xi, \quad (18)$$

where $\text{F}_2(a, b, b'; c, c'; x, y)$ stands for the Appell's hypergeometric function of the second kind [23, eq. (9.180.2)], and $\mathcal{L}_I(\xi r^{\alpha})$ is given in (7)-(8).

Proof: Plugging (6) into (17), and resorting to

$$\text{F}_2\left(a, b, b'; c, c'; x, y\right) = \frac{1}{\Gamma(b')}\int_0^{\infty} t^{b'-1}e^{-t} \times \Psi_1\left(a, b; c, c'; x, yt\right) dt, \quad (19)$$

yields the desired result after some manipulations.

A hallmark of current-small cell systems in urban environments is that they are overwhelmingly interference-limited, where the downlink channels are severed by interference rather than by thermal noise, especially at the cell edge where the interference power is typically so much larger. In such a case, the average rate is limited by bandwidth rather than power. Therefore, the case of no noise (or infinite transmit power P) is of particular interest because it captures the scenario where the transmit power would not be a binding constraint over downlink communications.

Corollary 1 (Shadowed κ-μ, No Noise or Infinite P): The interference-limited ergodic rate of a typical mobile user on the downlink over shadowed κ-μ fading is

$$C^{S\kappa\mu,\infty}(\alpha) = \frac{\Omega}{\left(\frac{\mu\kappa}{m}+1\right)^m (1+\kappa)} \times \int_0^\infty \frac{\mathrm{F}_2\left(\mu+1, m, 1; 2, \mu; \frac{\mu\kappa}{\mu\kappa+m}, \frac{-\xi\Omega}{\mu(1+\kappa)}\right)}{1+\mathcal{A}^{S\kappa\mu}(\xi)} d\xi, \tag{20}$$

where

$$\mathcal{A}^{S\kappa\mu}(\xi) = \begin{cases} \sum_{k=1}^{m_I} \frac{\binom{m_I}{k}\Xi^k\xi^k {}_2\mathrm{F}_1\left(m_I, k-\frac{2}{\alpha}, k+1-\frac{2}{\alpha}, -\Xi\xi\right)}{\frac{\alpha k}{2}-1} - \\ \sum_{n=1}^{m_I-\mu_I} \frac{\binom{m_I-\mu_I}{n}\Theta^n\xi^n {}_2\mathrm{F}_1\left(m_I, n-\frac{2}{\alpha}, n+1-\frac{2}{\alpha}, -\Xi\xi\right)}{\frac{\alpha n}{2}-1}, \\ \qquad\qquad \mu_I \le m_I; \\ \sum_{n,k;(n,k)\neq(0,0)}^{m_I,\mu_I-m_I} \frac{\binom{\mu_I-m_I}{k}\binom{m_I}{n}\Theta^k\Xi^n\xi^{k+n}}{\frac{\alpha(n+k)}{2}-1} \mathrm{F}_1\Big(n+k-\frac{2}{\alpha}, \\ \mu_I-m_I, m_I, n+k+1-\frac{2}{\alpha}, -\Theta\xi, -\Xi\xi\Big), \quad \mu_I > m_I. \end{cases} \tag{21}$$

Proof: When noise is neglected, i.e., $\sigma^2 \simeq 0$ or the transmit power is not a binding constraint i.e., $P \simeq \infty$, then the expectation $\mathcal{E}_r\left[\exp\left(-\xi r^\alpha \frac{\sigma^2}{P}\right)\mathcal{L}_I^{S\kappa\mu}(\xi r^\alpha)\right] \underset{\sigma^2\simeq 0, P\simeq\infty}{\approx} \mathcal{E}_r\left[\mathcal{L}_I(\xi r^\alpha)\right]$ with respect to the distance r separating a typical user from its tagged BS with pdf $f_r(x) = 2\pi\lambda x e^{-\pi\lambda x^2}$ is expressed in closed form using [23, eq. (3.326.2)], thereby yielding the simplified expressions of the ergodic rate shown in (20).

Theorem 6: The average rate of a typical mobile user at a distance r from its serving BS over κ-μ fading is

$$C^{\kappa\mu}(\lambda,\alpha) = \frac{\Omega e^{-\kappa\mu}}{(1+\kappa)}\int_0^\infty \Psi_1\left(\mu+1, 1; 2, \mu; \mu\kappa, \frac{-\xi\Omega}{\mu(1+\kappa)}\right) \times \mathcal{E}_r\left[\exp\left(-\xi r^\alpha\frac{\sigma^2}{P}\right)\mathcal{L}_I^{\kappa\mu}(\xi r^\alpha)\right] d\xi, \tag{22}$$

where $\mathcal{L}_I(\xi r^\alpha)$ is given in (10).

Proof: The results follows after substituting (9) into (17) and applying

$$\Psi_1(a,b;c,c';x,y) = \frac{1}{\Gamma(b)}\int_0^\infty t^{b-1}e^{-t}\Psi_2(a,c,c';x,yt)\,dt. \tag{23}$$

Another rationale to get (22) starts from (18) and employs the following limit relation [34]:

$$\lim_{\epsilon\to 0}\mathrm{F}_2\left(\alpha, \frac{b'}{\epsilon}, b, c', c; \epsilon x, y\right) = \Psi_1(\alpha, b; c', c; b'x, y). \tag{24}$$

Corollary 2 (κ-μ, No Noise or Infinite P): The interference-limited ergodic rate of a typical mobile user and its serving BS over κ-μ fading is

$$C^{\kappa\mu,\infty}(\alpha) = \frac{\Omega e^{-\kappa\mu}}{(1+\kappa)}\int_0^\infty \frac{\Psi_1\left(\mu+1, 1; 2, \mu; \mu\kappa, \frac{-\xi\Omega}{\mu(1+\kappa)}\right)d\xi}{1+\mathcal{A}^{\kappa\mu}(\xi)}. \tag{25}$$

where $\mathcal{A}^{\kappa\mu}(\xi) = \frac{\mu_I(1+\kappa_I)^{\mu_I}}{e^{\kappa_I\mu_I}\Omega_I^{\mu_I}}\sum_{k=0}^\infty \frac{\left(\frac{\mu_I^2\kappa_I(1+\kappa_I)}{\Omega_I}\right)^k}{k!} \sum_{n=1}^{\mu_I+k} \frac{\binom{\mu_I+k}{n}\left(\frac{\xi\Omega_I}{\mu_I\kappa_I(1+\kappa_I)}\right)^n {}_2\mathrm{F}_1\left(\mu_I+k-2, n-\frac{2}{\alpha}, n+1-\frac{2}{\alpha}, -\frac{\xi\Omega_I}{\mu_I\kappa_I(1+\kappa_I)}\right)}{\frac{\alpha n}{2}-1}$.

Proof: The result follows from (22) after setting $\sigma^2 = 0$ and using [23, eq. (3.326.2)].

Corollary 3 (Rice Fading): An interesting case to be addressed here is the typical Rice model, which arises from the κ-μ fading when $\mu = 1$ and $\kappa = K$ where K is the Rice factor. The ergodic rate under Rice fading is obtained from (22) as

$$C^{Rice}(\lambda,\alpha) = \frac{\Omega e^{-K}}{1+K}\int_0^\infty \Psi_1\left(2, 1; 2, 1; K, \frac{-\xi\Omega}{1+K}\right) \times \mathcal{E}_r\left[\exp\left(-\xi r^\alpha\frac{\sigma^2}{P}\right)\mathcal{L}_I^{Rice}(\xi r^\alpha)\right] d\xi, \tag{26}$$

where

$$\mathcal{L}_I^{Rice}(\xi r^\alpha) = \exp\Bigg(-2\pi\lambda\frac{r^2e^{-K}}{\Omega_I}\sum_{k=0}^\infty\frac{\left(\frac{K(1+K)}{\Omega_I}\right)^k}{k!} \times \sum_{n=1}^{k+1}\frac{\binom{k+1}{n}\left(\frac{\xi\Omega}{K(1+K)}\right)^n}{\alpha n-2} {}_2\mathrm{F}_1 \times \left(k-1, n-\frac{2}{\alpha}, n+1-\frac{2}{\alpha}, \frac{-\xi\Omega_I}{K(1+K)}\right)\Bigg). \tag{27}$$

Theorem 7: The average rate of a typical mobile user at a distance r from its serving BS over η-μ fading is

$$C^{\eta\mu}(\lambda,\alpha) = \frac{2\Omega\eta^{\mu+1}}{\eta+1}\int_0^\infty \mathrm{F}_2\left(2\mu+1, \mu, 1; 2, \mu; \frac{-\xi\Omega\eta}{\mu(1+\eta)}, 1-\eta\right)\mathcal{E}_r \times \left[\exp\left(-\xi r^\alpha\frac{\sigma^2}{P}\right)\mathcal{L}_I^{\eta\mu}(\xi r^\alpha)\right] d\xi. \tag{28}$$

Proof: The result is obtained along the same lines of (18) by performing similar substitutions as in (11). Moreover, $\mathcal{L}_I^{\eta\mu}(\xi r^\alpha)$ is given in (10).

Corollary 4 (η-μ, No Noise or Infinite P): The interference-limited ergodic rate of a typical mobile user on the downlink

over η-μ fading is

$$C^{\eta\mu,\infty}(\alpha)=\frac{2\Omega\eta^{\mu+1}}{\eta+1}\int_0^{\infty}\times\frac{\mathrm{F}_2\left(2\mu+1,\mu,1;2,2\mu;\frac{-\xi\Omega\eta}{\mu(1+\eta)},1-\eta\right)}{1+\mathcal{A}^{\eta\mu}(\xi)}d\xi. \tag{29}$$

where

$$\mathcal{A}^{\eta\mu}(\xi)=\sum_{\substack{n,k\\(n,k)\neq(0,0)}}^{\mu_I,\mu_I}\frac{\binom{\mu_I}{k}\binom{\mu_I}{n}\eta_I^{-k}\left(\frac{\Omega_I\eta_I\xi}{\mu_I(1+\eta_I)}\right)^{n+k}}{\frac{\alpha(n+k)}{2}-1}\mathrm{F}_1\times\left(n+k-\frac{2}{\alpha},\mu_I,\mu_I,n+k+1-\frac{2}{\alpha},-\frac{\Omega_I\xi}{\mu_I(1+\eta_I)},-\frac{\Omega_I\eta_I\xi}{\mu_I(1+\eta_I)}\right).$$

Proof: Substituting (12) into (28) with $\sigma^2=0$ and using [23, eq. (3.326.2)] yield the desired result.

Theorem 8: The average ergodic rate of a typical mobile user over Nakagami-m fading is

$$C^{m}(\lambda,\alpha)=\int_0^{\infty}\frac{\left(1-\left(1+\frac{\Omega\xi}{m}\right)^{-m}\right)\mathcal{E}_r\left[e^{-\frac{\xi r^\alpha\sigma^2}{P}}\mathcal{L}_I^m\left(\xi r^\alpha\right)\right]}{\xi}d\xi, \tag{30}$$

where $\mathcal{L}_I^m(\xi r^\alpha)$ is given in (15).

Proof: The result is a special case of (20) when $m=\mu$. In this case, a reduction formula of the Appell's F_2 function is given in Appendix E. Alternatively, one can obtain (30) after plugging (14) into (17) and resorting to [23, eq. (7621.5)].

Corollary 5 (Nakagami-m, No Noise or Infinite P): The interference-limited ergodic rate of a typical mobile user on the downlink over Nakagami-m fading is obtained as

$$C^{m,\infty}(\alpha)=\int_0^{\infty}\frac{1-\left(1+\frac{\Omega\xi}{m}\right)^{-m}}{\xi\,{}_2\mathrm{F}_1\left(\frac{-2}{\alpha},m_I,1-\frac{2}{\alpha};-\frac{\Omega_I}{m_I}\xi\right)}d\xi. \tag{31}$$

The Rayleigh case reduces from (31) when $m=m_I=1$; a key result previously obtained in [1, Th. 3], under, however, a more involved expression that encompasses a two-fold integration.

Equations (20), (25), (29), and (31) show that if $\sigma^2\to 0$ (or the transmit power is not a binding constraint, i.e., $P=\infty$), the average rate in a single-tier cellular network is independent of the BS intensity. This result is in compliance with those disclosed in [1]. In terms of average spectral efficiency, the downlink SINR performance (in case of non-binding maximum transmit power constraint) is independent of the BS intensity. Therefore, interference management techniques such as frequency reuse, interference cancellation, MIMO communications, interference avoidance, inter-cell cooperation, etc., are indeed overriding in order to increase the average rate in interference-limited cellular networks.

V. Coverage Probability

The cellular coverage probability is defined as

$$P_{cov}(T)\triangleq\mathbb{P}\left(\mathrm{SINR}\geq T\right), \tag{32}$$

where T represents the minimum SINR value for reliable downlink connection.

Remark (Laplace Transform Inversion): The Laplace transform of the complementary cumulative distribution function (CCDF) of the SINR, that is $P_{cov}(T)=\mathbb{P}(\mathrm{SINR}\geq T)$, $T\geq 0$, is related to the Laplace transform of the SINR as follows

$$\begin{aligned}\mathcal{L}_{P_{cov}}(z)&=\int_0^{\infty}P_{cov}(y)e^{-zy}dy\\&\overset{(a)}{=}\left[P_{cov}(y)\frac{-e^{-zy}}{z}\right]_0^{\infty}-\int_0^{\infty}P'_{cov}(y)\frac{-e^{-zy}}{z}dy\\&\overset{(b)}{=}\frac{1-\mathcal{E}[e^{-z\mathrm{SINR}}]}{z}=\frac{1}{z}-\frac{M_{\mathrm{SINR}}(z)}{z},\end{aligned} \tag{33}$$

where equality (a) is due to integration by parts and equality (b) follows form the definition of the MGF. The SINR CCDF $P_{cov}(T)$ may be retrieved from its Laplace transform using the Euler characterization as [36, eq. (2)]

$$\begin{aligned}P_{cov}(T)&\triangleq\mathbb{P}\left(\mathrm{SINR}\geq T\right)\\&=\frac{2\,e^{bT}}{\pi}\int_0^{\infty}\mathrm{Re}\left[\mathcal{L}_{P_{cov}}(b+iu)\right]\cos(uT)du,\end{aligned} \tag{34}$$

where $i^2=-1$ and $b>0$ is such that $\mathcal{L}_{P_{cov}}$ has no singularities on or to the right of it. The above inversion may be carried numerically using the Abate and Whitt algorithm [36, eq. (15)]

$$P_{cov}(T)\simeq\frac{2^{-m}e^{A/2}}{T}\sum_{k=0}^{m}\binom{m}{k}\sum_{l=0}^{n+k}\frac{(-1)^l\mathrm{Re}\left[\mathcal{L}_{P_{cov}}\left(\frac{A+2i\pi l}{2T}\right)\right]}{l+\mathbf{1}\{l=0\}}, \tag{35}$$

with a typical choice of $A=18.4$, $m=11$, and $n=15$.

The following propositions provide the downlink SINR in cellular networks over the considered fading models.

Proposition 1: The coverage probability of a typical-randomly located mobile user in the general cellular network model of Section II over shadowed κ-μ fading is

$$\begin{aligned}P_{cov}^{S\kappa\mu}(T)=&\frac{2\,e^{bT}\Omega}{\pi\left(\frac{\mu\kappa}{m}+1\right)^m(1+\kappa)}\int_0^{\infty}\int_0^{\infty}\mathrm{Re}\\&\times\left[\Psi_1\left(\mu+1,m;2,\mu;\frac{-(b+iu)\xi\Omega}{\mu(1+\kappa)},\frac{\mu\kappa}{\mu\kappa+m}\right)\right]\\&\times\cos(uT)du\mathcal{E}_r\left[\exp\left(-\xi r^\alpha\frac{\sigma^2}{P}\right)\mathcal{L}_I^{S\kappa\mu}\left(\xi r^\alpha\right)\right]d\xi.\end{aligned} \tag{36}$$

Proof: Combining (33) and (34) and using (6) yield the result after some manipulations.

Proposition 2: The coverage probability of a typical randomly-located mobile user in the general cellular network model of Section II over κ-μ fading is

$$P_{cov}^{\kappa\mu}(T) = \frac{2\, e^{bT}\Omega e^{-\kappa\mu}}{\pi(1+\kappa)} \times \int_0^\infty \int_0^\infty \mathrm{Re}\left[\Psi_2\left(\mu+1;\, 2,\, \mu; \frac{-(b+iu)\xi\Omega}{\mu(1+\kappa)},\, \mu\kappa\right)\right] \times \cos(uT)du\mathcal{E}_r\left[\exp\left(-\xi r^\alpha \frac{\sigma^2}{P}\right)\mathcal{L}_I^{\kappa\mu}\left(\xi r^\alpha\right)\right]d\xi. \tag{37}$$

Proof: The result is obtained along the same lines of (36) with the difference of using (9).

As for η-μ fading, the result follows along the same lines of (37) with the use of the appropriate SINR's MGF expression given in (11). The result is omitted here for the sake of conciseness.

Proposition 3: In a Rician fading environment with parameters K and Ω, the coverage probability is given by

$$P_{cov}^{Rice}(T) = \frac{2\, e^{bT}e^{-K}\Omega}{\pi(1+K)}\int_0^\infty\int_0^\infty \mathrm{Re} \times \left[\Psi_2\left(2;\, 2,\, 1;\, \frac{-(b+iu)\xi\Omega}{1+K},\, K\right)\right]\cos(uT)\mathcal{E}_r \times \left[\exp\left(-\xi r^\alpha\frac{\sigma^2}{P}\right)\mathcal{L}_I^{Rice}\left(\xi r^\alpha\right)\right]du\; d\xi. \tag{38}$$

Proof: The coverage probability under Rician fading is derived from (37) by setting $\mu = 1$ and $\kappa = K$.

Proposition 4: In Nakagami-m, the coverage probability is given by

$$p_{cov}^{m}(T) = \frac{2\, e^{bT}\Omega}{m}\int_0^\infty\int_0^\infty \mathrm{Re} \times \left[{}_1\mathrm{F}_1\left(m+1,\, 2;\, \frac{-(b+iu)\Omega}{m}\xi\right)\right]\cos(uT)\mathcal{E}_r \times \left[\exp\left(-\xi r^\alpha\frac{\sigma^2}{P}\right)\mathcal{L}_I^{m}\left(\xi r^\alpha\right)\right]du\; d\xi. \tag{39}$$

Proof: Combining (33) and (34) and using (14) yield the desired result after some manipulations. Note that (39) could also be derived from (36) by setting $\mu = m$ and form (37) when $\kappa \to 0$ [20].

Under the commonly-used Rayleigh fading, the coverage probability follows from substituting (16) into (34). Resorting to the fact that

$$\int_0^\infty \mathrm{Re}\left[\exp(-(b+iu)\xi\Omega)\right]\cos(uT)du = \frac{e^{-b\xi\Omega}}{2}\delta[T-\Omega\xi], \tag{40}$$

where $\delta(\cdot)$ is the Dirac delta function, it follows that under Rayleigh fading, P_{cov} is given by

$$p_{cov}^{R}(T) = \Omega e^{bT}\int_0^\infty e^{-b\xi\Omega}\delta[T-\Omega\xi]\mathcal{E}_r \times\left[\exp\left(\frac{-\xi r^\alpha\sigma^2}{P}\right)\mathcal{L}_I\left(\xi r^\alpha\right)\right]d\xi = \mathcal{E}_r\left[\exp\left(-\frac{T}{\Omega}r^\alpha\sigma^2\right)\mathcal{L}_I\left(\frac{T}{\Omega}r^\alpha\right)\right]. \tag{41}$$

The last expression in (41) matches the well-known main result for Rayleigh fading in [1], validating once again the wider scope of our new analysis approach.

So far, we have been able to provide a unified framework for cellular networks performance through the derivation of average rate and coverage probability, two metrics that are agnostic towards the modulation scheme and the receiver type. However, to capture more system details, we aim in the following to extend our new stochastic geometry analysis framework to a tangible error performance metric, namely the BEP.

VI. Average BEP Under Gaussian Signaling Approximation

This section delves into fine wireless communication details trough BEP analysis. In the context of wireless networks, error probability performance has mainly been studied and conducted over additive white Gaussian noise (AWGN) or Gaussian-interference channels [26]. Without loss of generality, we focus on the BEP, denoted by $\mathcal{B}$, for coherent M-PSK (phase shift keying) and M-QAM (quadrature amplitude modulation) constellations given by [26], [37]

$$\mathcal{B} = \beta_M\sum_{p=1}^{\tau_M}\mathcal{E}\left[\mathrm{Q}\left(a_p\sqrt{\mathrm{SINR}}\right)\right], \tag{42}$$

where $\mathrm{Q}(\cdot)$ is the Gaussian Q-function [37, eq. (2.1.97)] and β_M, a_p, and τ_M are modulation-dependent parameters specified in [26] and [37]. All parameters in the BEP expression in (42) are deterministic, and the expression is derived based on the Gaussian distribution of the noise and interference. However, in the context of cellular networks, many research works have shown that the aggregate interference does not follow a Gaussian distribution [5], [38], [39], thereby rendering (42) obsolete.

One elegant solution for the exploitation of (42) in the error performance analysis in cellular networks is to assume that each transmitter randomly selects its transmitted symbol from a Gaussian constellation with unit variance, known as Gaussian signalling approximation, with the main idea of abstracting unnecessary system details (i.e., the interferers' transmitted symbols) [10], [11]. Besides its simplicity, this method accurately captures the symbol and bit error probabilities without compromising the modeling accuracy (i.e., does not change the distribution of the aggregate interference [10]). Hereafter, by exploiting the Gaussian signaling approximation, we provide the BEP performance of a typical mobile user on

the downlink under the considered channel models, namely shadowed κ-μ, κ-μ, η-μ, and all other related distributions.

A. General Case

Theorem 8: The average BEP of a cellular downlink over shadowed κ-μ fading is

$$\mathcal{B}^{S\kappa\mu}(\lambda,\alpha) = \frac{\beta_M \tau_M}{2} - \frac{\beta_M \Gamma(\mu+\frac{1}{2})\sqrt{\frac{\Omega}{\mu(1+\kappa)}}}{\sqrt{2}\pi\,\Gamma(\mu)\left(\frac{\mu\kappa}{m}+1\right)^m} \sum_{p=1}^{\tau_M} a_p \times \int_0^\infty \frac{\Psi_1\left(\mu+\frac{1}{2}, m; \frac{3}{2}, \mu; \frac{-a_p^2\xi\Omega}{2\mu(1+\kappa)}, \frac{\mu\kappa}{\mu\kappa+m}\right)}{\sqrt{\xi}} \times \mathcal{E}_r\left[\exp\left(-\xi r^\alpha \frac{\sigma^2}{P}\right)\mathcal{L}_I^{S\kappa\mu}\left(\xi r^\alpha\right)\right] d\xi. \quad (43)$$

Proof: See Appendix F.

Theorem 9: The average BEP of a cellular downlink over κ-μ fading is

$$\mathcal{B}^{\kappa\mu}(\lambda,\alpha) = \frac{\beta_M \tau_M}{2} - \frac{\beta_M \Gamma(\mu+\frac{1}{2}) e^{\kappa\mu}\sqrt{\frac{\Omega}{\mu(1+\kappa)}}}{\sqrt{2}\pi\,\Gamma(\mu)} \times \sum_{p=1}^{\tau_M} a_p \int_0^\infty \frac{\Psi_2\left(\mu+\frac{1}{2}; \frac{3}{2}, \mu; \frac{-a_p^2\Omega\xi}{2\mu(1+\kappa)}, \mu\kappa\right)}{\sqrt{\xi}} \times \mathcal{E}_r\left[\exp\left(-\xi r^\alpha \frac{\sigma^2}{P}\right)\mathcal{L}_I^{\kappa\mu}\left(\xi r^\alpha\right)\right] d\xi. \quad (44)$$

Proof: The result follows after recognizing that $\mathcal{B}^{\kappa\mu}(\lambda,\alpha) = \lim_{m\to\infty} \mathcal{B}^{S\kappa\mu}(\lambda,\alpha)$. Then, recalling (64) yields the desired result after some manipulations. Note that the same result could be obtained by following similar steps leading to (44) with one difference of using the integral representation of Ψ_2 in [34, eq. (40)]. Notice when $\mu = 1$ and $\kappa = K$ that (44) reduces to the BEP expression under Rice fading.

Theorem 10: The average BEP of a cellular downlink over η-μ fading is

$$\mathcal{B}^{\eta\mu}(\lambda,\alpha) = \frac{\beta_M \tau_M}{2} - \frac{\beta_M \eta^\mu \Gamma(2\mu+\frac{1}{2})\sqrt{\frac{\Omega\eta}{\mu}}}{\sqrt{2}\pi\,\Gamma(2\mu)} \sum_{p=1}^{\tau_M} a_p \int_0^\infty \times \frac{\Psi_1\left(2\mu+\frac{1}{2}, \mu; \frac{3}{2}, 2\mu; \frac{-a_p^2\xi\Omega\eta}{2\mu(1+\eta)}, 1-\eta\right)}{\sqrt{\xi}} \times \mathcal{E}_r\left[\exp\left(-\xi r^\alpha \frac{\sigma^2}{P}\right)\mathcal{L}_I^{\eta\mu}\left(\xi r^\alpha\right)\right] d\xi. \quad (45)$$

Proof: The average BEP over η-μ fading is obtained form (43) by setting $\underline{m} = \mu$, $\underline{\mu} = 2\mu$, and $\underline{\kappa} = \frac{1-\eta}{2\eta}$ in both the desired and interfering fading channels and performing the necessary simplifications.

Corollary 5: The average BEP for the downlink cellular communication links in general Nakagami-m fading is

$$\mathcal{B}^{m}(\lambda,\alpha) = \frac{\beta_M \tau_M}{2} - \frac{\beta_M \Gamma(m+\frac{1}{2})\sqrt{\frac{\Omega}{m}}}{\sqrt{2}\pi\,\Gamma(m)} \sum_{p=1}^{\tau_M} a_p \times \int_0^\infty \frac{{}_1\mathrm{F}_1\left(m+\frac{1}{2}, \frac{3}{2}; \frac{-a_p^2\xi\Omega}{2\,m}\right)}{\sqrt{\xi}} \mathcal{E}_r \times \left[e^{-\xi r^\alpha \frac{\sigma^2}{P}}\mathcal{L}_I^m\left(\xi r^\alpha\right)\right] d\xi. \quad (46)$$

Proof: The result follows from (43) by setting $m = \mu$ and using the Humbert Ψ_1 function reduction formulas given in Appendix D. Alternatively, plugging (14) into (42) and following the same steps of Appendix F yield the desired result.

Recently, the authors of [11] investigated the impact of Gaussian signalling under Nakagami-m and derived the corresponding error rates. Although the number of integrals in the obtained BEP expression in (46) is not reduced when compared to [11], our approach discards the necessity for integer m, an assumption made in [11] for the sake of tractability. In practical scenarios, however, the m parameter often takes non-integer values, as argued by [40]. Once again, the significance of this work is highlighted by its very wide scope.

It is worthwhile to notice that all the BEP expressions in (43)-(46) are characterized by the Laplace transforms of the aggregate interference $\mathcal{L}_I$ given in Section II, which are the same ones used to characterize the coverage probability and average rate. As far as computational complexity is concerned, the comparison with previous results is not legitimate since this work is the first of its kind addressing fading distributions other than Rayleigh and integer Nakgami-m fading. Yet, all the obtained BEP expressions, like those obtained in previous works [3], [5], [11], encompass a two-fold integration of common built-in functions. A single integral approximation of the BEP is only possible for the special case of $\alpha = 4$. Since that has been extensively investigated in the literature, we omit it for the sake of conciseness.

B. Special Case of No Noise and High Signal to Interference Ratio (SIR)

When interference dominates the noise (i.e., $\sigma^2 \longrightarrow 0$), the average BEP expressions under the different considered fading distributions follow from (43)-(46) after computing the expectation over the distance r using [23, eq. (3.326.2)]. We are not providing these expressions here since similar proof has been already shown in Section III. However, it is interesting to further push the analysis toward closed-form expressions for the BEP by considering the high SIR scenario. In this case, to simplify the analysis we assume that interference undergoes Nakagami-m fading and thus $\mathcal{L}_I$ is given by (15).

Assuming that the desired link undergoes shadowed κ-μ fading, then substituting (15) into (43) with $\sigma^2 = 0$ and averaging over r yields the interference-limited BEP expression

for shadowed κ-μ fading on the desired link and Nakagami-m fading on the interfering links as

$$\mathcal{B}^{S\kappa\mu}(\alpha) = \frac{\beta_M \tau_M}{2} - \frac{\beta_M \Gamma(\mu+\frac{1}{2})\sqrt{\frac{\Omega}{\mu(1+\kappa)}}}{\sqrt{2}\pi\,\Gamma(\mu)\left(\frac{\mu\kappa}{m}+1\right)^m} \sum_{p=1}^{\tau_M} a_p \times \int_0^\infty \frac{\Psi_1\left(\mu+\frac{1}{2}, m; \frac{3}{2}, \mu; \frac{-a_p^2\xi\Omega}{2\mu(1+\kappa)}, \frac{\mu\kappa}{\mu\kappa+m}\right)}{\sqrt{\xi}\,{}_2\mathrm{F}_1\left(\frac{-2}{\alpha}, m_I, 1-\frac{2}{\alpha}; -\frac{\Omega_I}{m_I}\xi\right)} d\xi. \quad (47)$$

In what follows, we define the average received SIR as $\mathrm{SIR} = \frac{\Omega}{\Omega_I}$ and derive closed-from BEP expressions under the considered fading models when $\mathrm{SIR} \to \infty$.

Corollary 1 (Shadowed κ-μ, High SIR): The high SIR interference-limited average BEP over shadowed κ-μ on the desired link and Nakagami-m fading on the interfering links is given by

$$\mathcal{B}^{S\kappa\mu,\infty}(\alpha) = \frac{\beta_M}{2\left(\frac{\mu\kappa}{m}+1\right)^m}\left(\sum_{p=1}^{\tau_M} \Psi_1\left(\mu, m; \frac{1}{2}, \mu; \frac{a_p^2\delta}{4\mu(1+\kappa)}, \frac{\mu\kappa}{\mu\kappa+m}\right) - \frac{\Gamma(\mu+\frac{1}{2})\sqrt{\frac{\delta}{\mu(1+\kappa)}}}{\Gamma(\mu)} \sum_{p=1}^{\tau_M} a_p \Psi_1\left(\mu+\frac{1}{2}, m; \frac{3}{2}, \mu; \frac{a_p^2\delta}{4\mu(1+\kappa)}, \frac{\mu\kappa}{\mu\kappa+m}\right)\right). \quad (48)$$

Proof: See Appendix G with $\delta = \frac{(\alpha-2)\Omega}{\Omega_I}$.

Corollary 2 (κ-μ, High SIR): If the desired signal fading is κ-μ distributed, the average BEP in the high SIR regime becomes

$$\mathcal{B}^{\kappa\mu,\infty}(\alpha) = \frac{\beta_M e^{\kappa\mu}}{2}\left(\sum_{p=1}^{\tau_M} \Psi_2\left(\mu; \frac{1}{2}; \mu\frac{a_p^2\delta}{4\mu(1+\kappa)}, \mu\kappa\right) - \frac{\Gamma(\mu+\frac{1}{2})\sqrt{\frac{\delta}{\mu(1+\kappa)}}}{\Gamma(\mu)} \sum_{p=1}^{\tau_M} a_p \Psi_2 \times \left(\mu+\frac{1}{2}; \frac{3}{2}, \mu; \frac{a_p^2\delta}{4\mu(1+\kappa)}, \mu\kappa\right)\right). \quad (49)$$

Proof: The proof starts from (48) and uses the limit relations in (64) and (65).

Corollary 3 (Nakagami-m, High SIR): The high SIR interference-limited average BEP when both the desired and interference channels undergo Nakagami-m fading reduces to

$$\mathcal{B}^{m,\infty}(\alpha) = \frac{\beta_M}{2}\left(\sum_{p=1}^{\tau_M} {}_1\mathrm{F}_1\left(m, \frac{1}{2}; \frac{a_p^2\delta}{4m}\right) - \frac{\Gamma(m+\frac{1}{2})\sqrt{\frac{\delta}{m}}}{\Gamma(m)} \times \sum_{p=1}^{\tau_M} a_p\ {}_1\mathrm{F}_1\left(m+\frac{1}{2}, \frac{3}{2}; \frac{a_p^2\delta}{4m}\right)\right) = \frac{\beta_M\Gamma(m+\frac{1}{2})}{2\sqrt{\pi}} \sum_{p=1}^{\tau_M} \mathrm{U}\left(m, \frac{1}{2}, \frac{a_p^2\delta}{4m}\right), \quad (50)$$

where $\mathrm{U}(a, b; z)$ stands for the Tricomi confluent hypergeometric function [23, eq. (9.211.1)].

Proof: See Appendix H.

Notice that (50) also follows from (48) by setting $m = \mu$ and using the Humbert Ψ_1 function reduction formulas given in Appendix D, thereby corroborating again the correctness of our derivations.

Remark: Inspecting (50) reveals that the error probability tends to decrease as δ and/or m increase, meanwhile it is independent of m_I. Along the same lines, both $\mathcal{B}^{S\kappa\mu,\infty}$ and $\mathcal{B}^{\kappa\mu,\infty}$ are independent of m_I. However, trends against κ and μ which are rather intricate to investigate analytically will be assessed through simulations in the next section.

VII. Numerical and Simulation Results

In this section, numerical examples are shown to substantiate the accuracy of the new unified mathematical framework and to confirm its potential for analyzing cellular networks. All the results shown here have been analytically obtained by the direct evaluation of the expressions developed in this paper. Additionally, using the procedure described in [17, Sec. V-a], Monte Carlo simulations have been performed to validate the derived expressions, and are also presented in some figures, showing an excellent agreement with the analytical results.

Fig. 1 compares the average rate and average BEP for the κ-μ shadowed fading across a wide range of channel parameters (m, κ, μ). In Fig. 1 (a), $C^{S\kappa\mu}$ is represented as a function of the LOS component in the received wave clusters κ for different values of the μ parameter. We note that a rich scattering (large μ) achieves a higher rate with diminishing returns as κ increases, since increasing μ in the strong LOS scenario has little effect as the performance is dominated by the LOS component. When $m = \mu$, the κ-μ shadowed fading distribution boils down to the Nakagami-m distribution, whence the average rate's independency of κ.

The impact of shadowed LOS components on performance can be observed in Fig. 1 (b), where the average rate under κ-μ shadowed fading is presented as a function of the average SNR for different values of m and considering, respectively, small ($\kappa = 1$) and large ($\kappa = 20$) LOS components. It can be observed that performance improves with small LOS components ($\kappa = 1$) if the latter are affected by heavy shadowing (small m). However, when the shadowing is mild, large LOS components ($\kappa = 20$) always improve the average rate. In fact, small m indicates highly fluctuating dominant components, which decrease both the received signal and the aggregate interference powers thereby increasing the SINR level and ultimately achieving higher rates. Conversely, when m is large, the shadowing on the dominant components subsides and κ-μ shadowed fading reduces to κ-μ fading. Moreover, light shadowing always yields higher interference power thereby deteriorating the received SINR level as well as the average rate. Fig. 1 (b) also compares the average rate for various BS densities λ. It can be seen that the average rate of a sparse network ($\lambda \leq 10^{-4}$) is much lower than that of a dense network ($\lambda \geq 10^{-2}$). For example the average average rate is about 0.02 for $\lambda = 10^{-4}$ and 1 for $\lambda = 10^{-2}$ with $m = 0.5$, $\kappa = 20$ and $\mathrm{SNR} = 15$ dB.

Fig. 1 (c) plots the average BEP of the downlink with coherent QPSK ($M = 4$) under shadowed κ-μ fading on

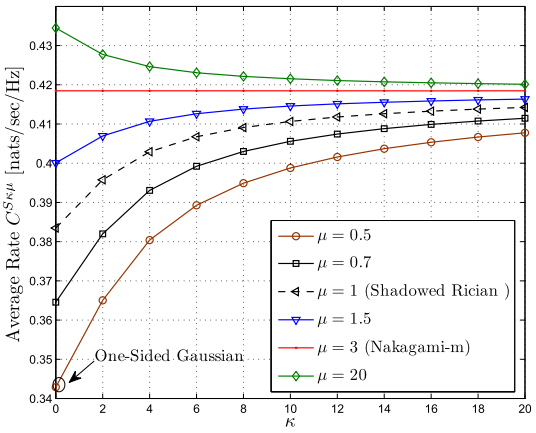

(a) $C^{S\kappa\mu}$ versus κ for $m = m_I = 3$, and $\mu_I = 1$.

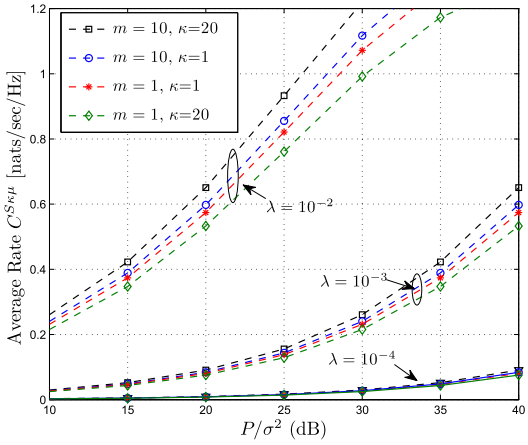

(b) $C^{S\kappa\mu}$ versus SNR for different values of $\kappa = \kappa_I$ and $m = m_I$ with $\mu = \mu_I = 2$.

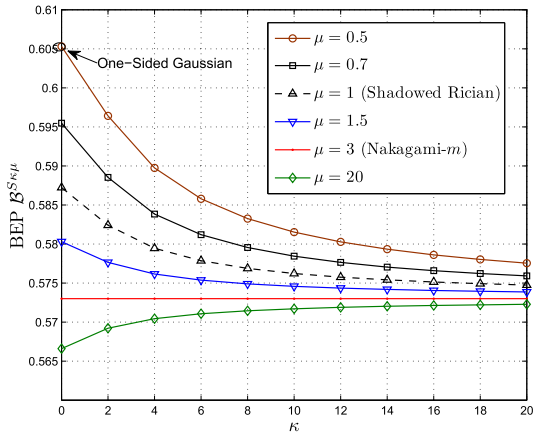

(c) $\mathcal{B}^{S\kappa\mu}$ versus κ for $m = m_I = 3$, $\mu_I = 1$, and $M = 4$.

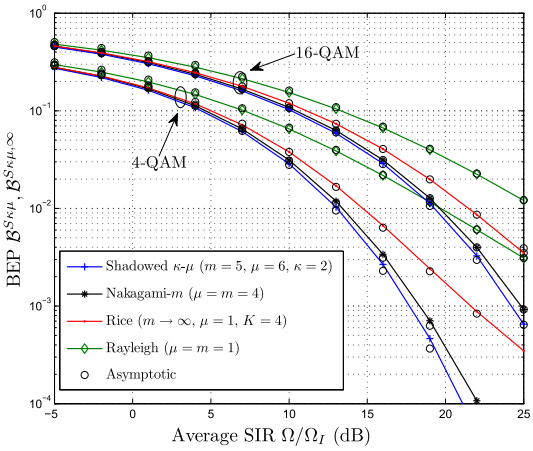

(d) $\mathcal{B}^{S\kappa\mu}$ and $\mathcal{B}^{S\kappa\mu,\infty}$ with Rayleigh interference versus SIR for $M \in \{4, 16\}$.

Fig. 1. Performance of downlink transmission over shadowed κ-μ fading. Setup: $\Omega_I = \Omega$, $\kappa_I = \kappa$, $\lambda = 10^{-4}$, and $\alpha = 3$.

both the desired and interfering links. As can be seen, a strong dominant LOS component (large κ) and rich scattering (large μ) collectively improve the error performance. The figure also shows that Rician fading on the useful link has higher performance than the Rayleigh fading due to the LOS path.

Fig. 1 (d) shows the average BEP versus the received SIR for various shadowed κ-μ fading environments in downlink. Recall that although the Rician model represents a LOS (and better) channel than the Rayleigh model, the large SNR tails of the Rician distribution always have the same decay rate as (i.e., are parallel to) the tails of the Rayleigh distribution (reflecting the diversity order of the channel). At high SIR, the asymptotic expansion in (48) matches very well its exact counterpart, which confirms the validity of our mathematical analysis for different parameter settings.

In Figs. 2 (a)-(d), the performance of downlink transmission over κ-μ and η-μ fading is presented.

Fig. 2 (a) depicts the ergodic rate $C^{\kappa\mu}$ under the κ-μ fading model. Since the shadowing can be neglected in this case, any increase in the power of the dominant components is obviously favorable for the channel capacity. It is therefore straightforward to see that increasing the parameter κ implies increasing the ergodic rate since a higher LOS power implies improving the capacity of the κ-μ channel.

Fig. 2 (b) compares the average rate under κ-μ fading versus the BS density λ for different values of the μ parameter. As conjectured in Corollay 1, the network performance is invariant of the network density in an interference-limited condition (large BS intensity). The results show that the rate saturation may happen at certain network density required to obtain sufficiently larger interference power than the noise. In fact, at high SNR, the saturation regime is reached at $\lambda = 10^{-2}$, compared to $\lambda \geq 10^{-1}$ in the low SNR regime. In practice, installing more BSs is beneficial to the user performance up to a density point, after which further densification turns out to be extremely ineffective due to faster growth of interference compared to useful signal. This highlights the cardinal importance of interference mitigation, coordination among neighboring cells and local spatial scheduling.

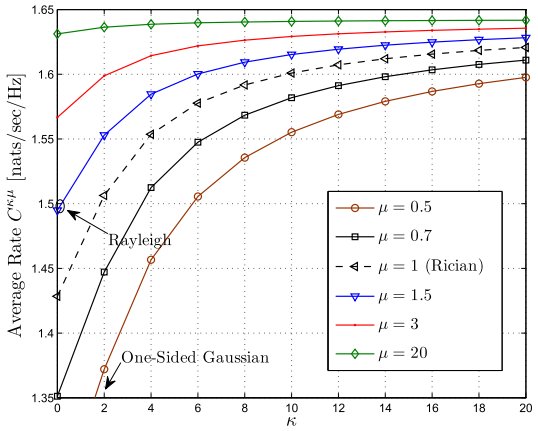

(a) $C^{\kappa\mu}$ versus κ with $\mu_I = 1$.

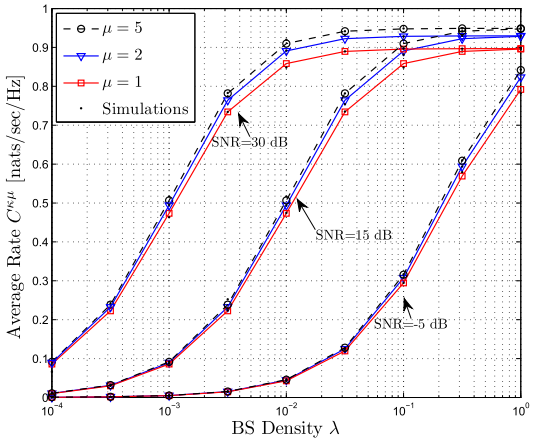

(b) $C^{\kappa\mu}$ versus BS density λ for different values of $\mu = \mu_I$ with $\kappa = 1.5$.

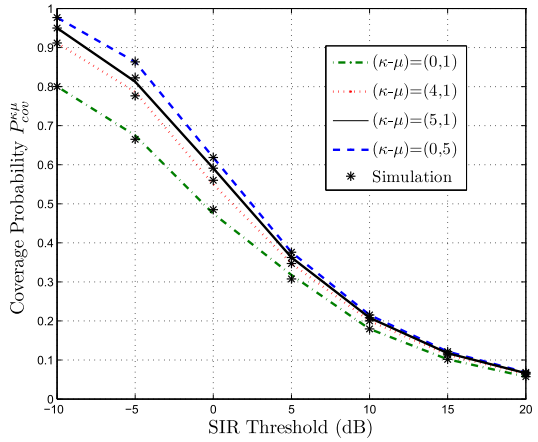

(c) SIR coverage probability $P_{cov}^{\kappa\mu}$.

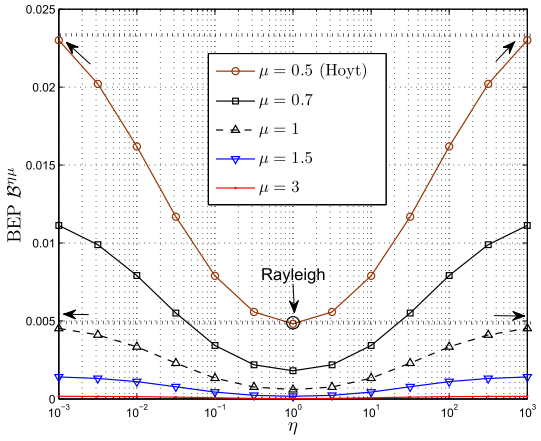

(d) $\mathcal{B}^{\eta\mu}$ versus η for $M = 4$ with $\mu_I = 1$.

Fig. 2. Performance of downlink transmission over κ-μ and η-μ fading. Setup: $\Omega_I = \Omega$, $\kappa_I = \kappa$, $\lambda = 10^{-4}$, and $\alpha = 3$.

Fig. 2 (c) plots the coverage probability versus the SIR threshold for different fading environments contained within the κ-μ model. It can be seen that both μ and κ have impact on the coverage probability with a more pronounced impact for the cluster number μ, especially for small κ, a behavior previously observed in Fig. 1 (a).

Fig. 2 (d) depicts the interference-limited average BEP for η-μ fading, which is, as expected, symmetrical on a logarithmic scale around the minimum value of the average BEP at $\eta = 1$ regardless of the number of clusters μ. In the same figure, we have specified the limit cases for $\eta \to 0$ and $\eta \to \infty$. When $\mu = 0.5$, the η-μ model collapses into the one-sided Gaussian model for $\eta = 0$ or $\eta \to \infty$, whereas for $\eta = 1$, it collapses into the Rayleigh model. When $\mu = 1$, the η-μ is reduced to the Rayleigh case for $\eta = 0$ or $\eta \to \infty$. Both the Rayleigh and one-sided Gaussian BEP values are illustrated by horizontal dotted and dashed lines, respectively.

In Fig. 1 and Fig. 2, please note that we have identified in the figure legends or with rounded circles the performance curves or points, respectively, of some particular fading distributions that simply reduce from the shadowed κ-μ, the κ-μ, and the η-μ models.

VIII. Conclusion

In this paper a novel mathematical methodology for performance evaluation on the downlink of cellular networks over fading channels is presented. The proposed approach exploits results from stochastic geometry for the computation of the SINR's MGF, which is shown to be conveniently formulated as a function of a desired-user fading dependent term and the Laplace transform of the interference. By capitalizing on this mathematical formulation, we have been able to obtain two-fold integral expressions for the ergodic rate, the coverage probability, and the tangible decoding error probability for various fading distributions. Remarkably, the proposed framework accommodates generic fading distribution models including shadowed κ-μ, κ-μ, and η-μ that account for LOS/NLOS and shadowed fading. Our results provide useful insights into the coverage, throughput, and BEP performance in complex fading environments and shed new lights on the prominent impact of DSCs and shadowed DSCs propagation on cellular networks. Finally, this new framework is flexible to capture several fading conditions ranging from deterministic and favorable Rician to severely shadowed and Rayleigh fading. Future work possibilities relying on this new modeling paradigm

are tremendous and include without limitation the extension to multi-tier heterogeneous networks (HetNet)s with arbitrary numbers of tiers having different densities and transmit powers. Moreover, the developed baseline model provides new powerful tools to analyze other network architectures such that device-to-device (D2D) and MIMO-enabled networks.

APPENDIX

A. Proof of Lemma 1

Given the SINR $= \frac{hr^{-\alpha}}{\frac{\sigma^2}{P}+I(r)}$, its MGF, defined as $M_{\mathrm{SINR}}(s) \triangleq \mathcal{E}_{r,h,I}\left[\exp\left(-s\mathrm{SINR}\right)\right]$, is evaluated as

$$\begin{aligned} M_{\mathrm{SINR}}(s) &= \mathcal{E}_{r,h}\left[\int_0^\infty \exp\left(-\frac{shr^{-\alpha}}{y}\right) f_{I+\frac{\sigma^2}{P}}(y)dy\right] \\ &= \mathcal{E}_{r,h}\left[\mathcal{L}_{\frac{1}{I+\frac{\sigma^2}{P}}}\left(shr^{-\alpha}\right)\right] \\ &\overset{(a)}{=} 1 - 2\mathcal{E}_r\Bigg[\sqrt{sr^{-\alpha}}\int_0^\infty \mathcal{E}_h\left[\sqrt{h}\mathrm{J}_1\left(2\sqrt{shr^{-\alpha}}\xi\right)\right] \\ &\quad \times \mathcal{L}_{I+\frac{\sigma^2}{P}}(\xi^2)d\xi\Bigg], \end{aligned} \tag{51}$$

where (a) follows from applying [32, Th. 1] and $\mathrm{J}_1(\cdot)$ is the Bessel function of the first kind and first order [23, eq. (8.402)]. Then Lemma 1 is obtained by a change of variable relabeling $\xi r^{-\frac{\alpha}{2}}$ as ξ, while taking into account the linearity and the time shifting properties of the Laplace transform implying that $\mathcal{L}_{I+\frac{\sigma^2}{P}}(x) = e^{-\frac{\sigma^2}{P}x}\mathcal{L}_I(x)$.

B. Proof of $M_{SINR}^{S\kappa\mu}$ and $\mathcal{L}_I^{S\kappa\mu}$

After applying (5), the expectation over shadowed κ-μ fading using the distribution in (1) can be calculated as

$$\begin{aligned} \mathcal{E}_h\left[\sqrt{h}\mathrm{J}_1\left(2\sqrt{sh}\xi\right)\right] &= A\int_0^\infty y^{\mu-\frac{1}{2}}e^{-By}\mathrm{J}_1\left(2\sqrt{sy}\xi\right) \\ &\quad \times {}_1\mathrm{F}_1\left(m,\mu,Cy\right)dy \end{aligned} \tag{52}$$

where we denote $A = \frac{\mu^\mu m^m(1+\kappa)^\mu}{\Gamma(\mu)\Omega^\mu(\mu\kappa+m)^m}$, $B = \frac{\mu(1+\kappa)}{\Omega}$, and $C = \frac{\mu^2\kappa(1+\kappa)}{\Omega(\mu\kappa+m)}$. Recalling the Bessel $\mathrm{J}_\nu(\cdot)$ representation through the more general confluent hypergeometric function ${}_1\mathrm{F}_1(\cdot)$ given by

$$\mathrm{J}_\nu(z) = \frac{z^\nu}{2^\nu\Gamma(\nu+1)}\lim_{a\to\infty}{}_1\mathrm{F}_1\left(a,\nu+1;\frac{-z^2}{4a}\right), \tag{53}$$

then it follows that

$$\begin{aligned} &\mathcal{E}_h\left[\sqrt{h}\mathrm{J}_1\left(2\sqrt{sh}\xi\right)\right] \\ &= A\sqrt{s}\xi\lim_{a\to\infty}\int_0^\infty y^\mu e^{-By}{}_1\mathrm{F}_1 \\ &\quad \times\left(a,2,\frac{-s\xi^2}{a}y\right){}_1\mathrm{F}_1\left(m,\mu,Cy\right)dy \\ &\overset{(a)}{=} \frac{A\Gamma(\mu+1)\sqrt{s}}{B^{\mu+1}}\xi\lim_{a\to\infty}\mathrm{F}_2 \\ &\quad \times\left(\mu+1,a,m,2,\mu;\frac{-s\xi^2}{aB},\frac{C}{B}\right) \\ &\overset{(b)}{=} \frac{A\Gamma(\mu+1)}{B^{\mu+1}}\sqrt{s}\xi\Psi_1 \\ &\quad \times\left(\mu+1,m;2,\mu;\frac{-s\xi^2}{B},\frac{C}{B}\right), \end{aligned} \tag{54}$$

where (a) follows from recognizing Appell's F_2 representation [34, eq. (27)]

$$\begin{aligned} &\mathrm{F}_2\left(a,b,b',c,c';\frac{w}{p},\frac{z}{p}\right) \\ &= \frac{p^a}{\Gamma(a)}\int_0^\infty x^{a-1}e^{-px}{}_1\mathrm{F}_1(b,c,wx) \\ &\quad \times{}_1\mathrm{F}_1\left(b',c',xz\right)dx, \quad \mathrm{Re}(a),\ \mathrm{Re}>0, \end{aligned} \tag{55}$$

and (b) is obtained by limit (confluence) formula [34]

$$\lim_{\epsilon\to0}\mathrm{F}_2\left(\alpha,\frac{b'}{\epsilon},b,c',c;\epsilon x,y\right) = \Psi_1\left(\alpha,b;c',c;b'x,y\right). \tag{56}$$

Finally substituting (54) into (5) and carrying out the change of variable relabeling ξ^2 as ξ yield the desired result after some manipulations.

The Laplace transform of the aggregate interference from the interfering BSs received at the tagged user under κ-μ shadowed fading, denoted as $\mathcal{L}_I^{S\kappa\mu}(\xi)$, is obtained as

$$\begin{aligned} \mathcal{L}_I(\xi) &= \mathcal{E}_{\Psi,h}\left[\exp\left(-\xi\sum_{i\in\Psi^{(\backslash0)}}h_i r_i^{-\alpha}\right)\right] \\ &\overset{(a)}{=} \exp\left(-2\pi\lambda\int_r^\infty\left(1-\mathcal{E}_h[\exp\left(-\xi hv^{-\alpha}\right)]\right)vdv\right) \\ &\overset{(b)}{=} \exp\Bigg(-2\pi\lambda\int_r^\infty\Bigg(1-\frac{\mu_I^{m_I}m_I^{m_I}(1+\kappa_I)^{\mu_I}}{\Omega_I^{\mu_I}(\mu_I\kappa_I+m_I)^{m_I}} \\ &\quad \times\frac{\left(\xi v^{-\alpha}+\frac{\mu_I(1+\kappa_I)}{\Omega_I}\right)^{m_I-\mu_I}}{\left(\xi v^{-\alpha}+\frac{\mu_I(1+\kappa_I)}{\Omega_I}\frac{m_I}{\mu_I\kappa_I+m_I}\right)^{m_I}}\Bigg)vdv\Bigg), \end{aligned} \tag{57}$$

where (a) follows from independence between Ψ and h_i and the probability generation functional (PGFL) of the PPP [27] and (b) follows from the MGF of h_i under shadowed κ-μ fading recently derived in [20, eq. (5)]. Further by letting $x \longleftarrow r^\alpha v^{-\alpha}$ in (57), the latter is obtained as

$$\begin{aligned} \mathcal{L}_I^{S\kappa\mu}(\xi r^\alpha) &= \exp\Bigg(-2\pi\lambda\frac{r^2}{\alpha}\int_0^1 x^{-\frac{2}{\alpha}-1} \\ &\quad \times\left(1-\frac{\left(1+\frac{\mu_I(1+\kappa_I)}{\Omega_I}\xi x\right)^{m_I-\mu_I}}{\left(1+\frac{(\mu_I\kappa+m_I)\Omega_I}{m_I\mu_I(1+\kappa_I)}\xi x\right)^{m_I}}\right)dx\Bigg), \end{aligned} \tag{58}$$

when $\mu_I \le m_I$, and in case of $\mu_I \ge m_I$, it can be calculated as

$$\begin{aligned} \mathcal{L}_I^{S\kappa\mu}(\xi r^\alpha) &= \exp\Bigg(-2\pi\lambda\frac{r^2}{\alpha}\int_0^1 x^{-\frac{2}{\alpha}-1} \\ &\quad \times\left(1-\frac{1}{\left(1+\frac{\mu_I(1+\kappa_I)}{\Omega_I}\xi x\right)^{\mu_I-m_I}\left(1+\frac{(\mu_I\kappa+m_I)\Omega_I}{m_I\mu_I(1+\kappa_I)}\xi x\right)^{m_I}}\right)dx\Bigg). \end{aligned} \tag{59}$$

Let $\Theta = \frac{\mu_I(1+\kappa_I)}{\Omega_I}$ and $\Xi = \frac{(\mu_I\kappa_I+m_I)\Omega_I}{m_I\mu_I(1+\kappa_I)}$. Then applying binomial expansion on $(1+\Xi\xi x)^{m_I} - (1+\Theta\xi x)^{m_I-\mu_I} =$

$\sum_{k=1}^{m_I}\binom{m_I}{k}\Xi^k\xi^k - \sum_{n=1}^{m_I-\mu_I}\binom{m_I-\mu_I}{n}\Theta^n\xi^n$ in the numerator of (58) and on $(1+\Xi\xi x)^{m_I}(1+\Theta\xi x)^{m_I-\mu_I} = \sum_{k=0}^{m_I}\sum_{n=0}^{m_I-\mu_I}\binom{m_I}{k}\binom{m_I-\mu_I}{n}\Xi^k\Theta^n x^{k+n}$ in the numerator of (59), we obtain [4]

$$\mathcal{L}_I^{S\kappa\mu}(\xi r^\alpha) = \exp\Bigg(-2\pi\lambda\frac{r^2}{\alpha}\Bigg(\sum_{k=1}^{m_I}\binom{m_I}{k}\Xi^k\xi^k \times\int_0^1\frac{x^{k-\frac{2}{\alpha}-1}}{(1+\Xi\xi x)^m}dx - \sum_{n=1}^{m_I-\mu_I}\binom{m_I-\mu_I}{n}\Theta^n\xi^n \times\int_0^1\frac{x^{n-\frac{2}{\alpha}-1}}{(1+\Xi\xi x)^m}dx\Bigg)\Bigg), \quad \text{when } \mu_I\le m_I, \tag{60}$$

and

$$\mathcal{L}_I^{S\kappa\mu}(\xi r^\alpha) = \exp\Bigg(-2\pi\lambda\frac{r^2}{\alpha}\sum_{n,k;(n,k)\neq(0,0)}^{m_I,\mu_I-m_I}\binom{\mu_I-m_I}{k}\binom{m_I}{n}\Theta^k\Xi^n \times\xi^{k+n}\int_0^1\frac{x^{k+n-\frac{2}{\alpha}-1}}{(1+\Theta\xi x)^{\mu_I-m_I}(1+\Xi\xi x)^{m_I}}dx\Bigg), \quad \text{when } \mu_I\ge m_I. \tag{61}$$

Closed-form expressions of (60) and (61) are obtained after recognizing that

$${}_2\mathrm{F}_1(a,b;c;x) = \frac{\Gamma(c)}{\Gamma(b)\Gamma(c-b)}\int_0^1 t^{b-1}(1-t)^{c-b-1}\times(1-tx)^{-a}dt, \quad \mathrm{Re}(c)>\mathrm{Re}(b)>0, \tag{62}$$

and

$$\mathrm{F}_1(a,b,b';c;w,z) = \frac{\Gamma(a)}{\Gamma(c)\Gamma(c-a)}\int_0^1 t^{a-1}(1-t)^{c-a-1}\times(1-tw)^{-b}(1-tz)^{-b'}dt, \quad \mathrm{Re}(a)>0, \tag{63}$$

which completes the proof and provide explicitly the $\mathcal{L}_I^{S\kappa\mu}(\xi)$ as shown in *Theorem 1*.

C. Proof of $M_{SINR}^{\kappa\mu}$ and $\mathcal{L}_I^{\kappa\mu}$

The κ-μ fading arises from the shadowed κ-μ fading as $m\to\infty$. Accordingly, it follows that $M_{\mathrm{SINR}}^{\kappa\mu} = \lim_{m\to\infty} M_{\mathrm{SINR}}^{S\kappa\mu}$, and $\mathcal{L}_I^{\kappa\mu} = \lim_{m_I\to\infty}\mathcal{L}_I^{S\kappa\mu}$. As far as $M_{\mathrm{SINR}}^{\kappa\mu}$ is concerned, the desired result follows by applying the following properties:

$$\lim_{\epsilon\to 0}\Psi_1\left(a,\frac{b}{\epsilon};c,c';\epsilon w,z\right) = \Psi_2(a;c,c';bw,z), \tag{64}$$

and

$$\lim_{a\to\infty}\left(\frac{x}{a}+1\right)^{-a} = e^{-x}, \tag{65}$$

where (65) is the well-known limit that defines the exponential function.

[4]Note that the obtainment of (60) and (61) inflicts the quantities m_I and μ_I to be integer valued.

Regarding $\mathcal{L}_I^{\kappa\mu}$, the specialization from $\mathcal{L}_I^{S\kappa\mu}$ is not straightforward and requires further manipulations. The proof tracks the proof of $\mathcal{L}_I^{S\kappa\mu}$ up until step (a) of (57). Then,

$$\begin{aligned}\mathcal{L}_I^{\kappa\mu}(\xi) &\overset{(a)}{=} \exp\Bigg(-2\pi\lambda\int_r^\infty \mathcal{E}_h\Big[\xi h v^{-\alpha}\exp\left(-\xi h v^{-\alpha}\right)\\ &\quad\times{}_1\mathrm{F}_1\left(1,2;\xi h v^{-\alpha}\right)\Big]v dv\Bigg)\\ &\overset{(b)}{=} \exp\Bigg(-2\pi\lambda\xi\frac{\mu_I(1+\kappa_I)^{\frac{\mu_I+1}{2}}}{e^{\kappa_I\mu_I}\Omega_I^{\frac{\mu_I+1}{2}}\kappa_I^{\frac{\mu_I-1}{2}}}\\ &\quad\times\int_r^\infty\frac{v^{-\alpha+1}}{\left(\xi v^{-\alpha}+\frac{\mu_I(\kappa_I+1)}{\Omega_I}\right)^{\frac{\mu_I-1}{2}}}\\ &\quad\times\int_0^\infty x^{\frac{\mu_I+1}{2}}e^{-x}{}_1\mathrm{F}_1\left(1,2;\frac{\xi v^{-\alpha}}{\xi v^{-\alpha}+\frac{\mu_I(\kappa_I+1)}{\Omega_I}}x\right)\\ &\quad\times\mathrm{I}_{\mu_I-1}\left(2\mu_I\sqrt{\frac{\kappa_I(1+\kappa_I)x}{\Omega_I\left(\xi v^{-\alpha}+\frac{\mu_I(\kappa_I+1)}{\Omega_I}\right)}}\right)dx dv\Bigg),\end{aligned} \tag{66}$$

where (a) follows from using the relation $(1-e^{-x})/x = e^{-x}{}_1\mathrm{F}_1(1,2;x)$ and (b) follows from the κ-μ distribution of h_i given in (2) and carrying out the change of variable $x = h\left(\xi v^{-\alpha}+\frac{\mu_I(\kappa_I+1)}{\Omega_I}\right)$.

$$\begin{aligned}\mathcal{L}_I^{\kappa\mu}(\xi r^\alpha) &\overset{(c)}{=} \exp\Bigg(-2\pi\lambda\frac{\mu_I^2(1+\kappa_I)^{\mu_I}}{e^{\kappa_I\mu_I}\Omega_I^{\mu_I}}\int_0^1\frac{\xi v^{-\alpha+1}}{\left(\xi x+\frac{\mu_I(\kappa_I+1)}{\Omega_I}\right)^{\mu_I-1}}\\ &\quad\times\Psi_1\left(\mu_I+1,1;\mu_I,2;\frac{\mu_I^2\kappa_I(1+\kappa_I)}{\Omega_I\left(\xi x+\frac{\mu_I(\kappa_I+1)}{\Omega_I}\right)},\right.\\ &\quad\left.\times\frac{\xi x}{\xi x+\frac{\mu_I(\kappa_I+1)}{\Omega_I}}\right)dx\Bigg)\\ &\overset{(d)}{=} \exp\Bigg(-2\pi\lambda\frac{r^2\mu_I^2(1+\kappa_I)^{\mu_I}}{\alpha e^{\kappa_I\mu_I}\Omega_I\mu_I}\sum_{k=0}^\infty\frac{(\mu_I+1)_k\left(\frac{\mu_I^2\kappa_I(1+\kappa_I)}{\Omega_I}\right)^k}{k!(\mu_I)_k(\mu_I+k)}\\ &\quad\times\int_0^1\frac{x^{-\frac{2}{\alpha}-1}\left(\left(\frac{\xi x}{\frac{\mu_I(\kappa_I+1)}{\Omega_I}}+1\right)^{\mu_I+k}-1\right)}{\left(\xi x+\frac{\mu_I(\kappa_I+1)}{\Omega_I}\right)^{\mu_I+k-2}}dx\Bigg)\\ &\overset{(e)}{=} \exp\Bigg(-2\pi\lambda\frac{r^2\mu_I^2(1+\kappa)^{\mu_I}}{\alpha e^{\kappa_I\mu_I}\Omega_I^{\mu_I}}\sum_{k=0}^\infty\frac{(\mu_I+1)_k\left(\frac{\mu_I^2\kappa_I(1+\kappa_I)}{\Omega_I}\right)^k}{k!(\mu_I)_k(\mu_I+k)}\\ &\quad\times\sum_{n=1}^{\mu_I+k}\frac{\binom{\mu_I+k}{n}\left(\frac{\xi\Omega_I}{\mu_I\kappa_I(1+\kappa_I)}\right)^n}{n-\frac{2}{\alpha}}{}_2\mathrm{F}_1\Bigg(\mu_I+k-2,\\ &\quad n-\frac{2}{\alpha},n+1-\frac{2}{\alpha},\frac{-\xi\Omega_I}{\mu_I\kappa_I(1+\kappa_I)}\Bigg)\Bigg),\end{aligned} \tag{67}$$

In (67), (c) results in the same line of (54) after using $\mathrm{I}_{\nu}(z) = \frac{z^{\nu}}{2^{\nu}\Gamma(\nu+1)} \lim_{a\to\infty} {}_1\mathrm{F}_1\left(a, \nu+1; \frac{z^2}{4\,a}\right)$ followed by the change of variable $x = \left(\frac{r}{v}\right)^{\alpha}$. The aggregate interference under κ-μ still needs manipulations as to solve the integral involving the Humbert function obtained after (c). To this end, we resort in (d) to the the series expansion of the Humbert function Ψ_1 given by [34]

$$\Psi_1\big(a, b; c, c'; x, y\big) = \sum_{k=0}^{\infty} \frac{(a)_k}{k!(c')_k} y^k {}_2\mathrm{F}_1(a+k, b, c; x), \quad |x|<1, \tag{68}$$

where $(a)_n$ denote the Pochhammer symbol, along with the reduction formulas of the Gauss hypergeometric function ${}_2\mathrm{F}_1(\cdot)$ given in [23, eq. (9.121.5)]. Finally (e) follows from using to the binomial expansion and recognising (62), thereby leading the desired result after some manipulations.

D. Proof of M^m_{SINR} and $\mathcal{L}^m_I$

When $m = \mu$, it holds that

$$\begin{aligned}
&\Psi_1\left(m+1, m; 2, m; \frac{-s\xi\Omega}{m(1+\kappa)}, \frac{m\kappa}{m\kappa+m}\right) \\
&\overset{(a)}{=} \lim_{\epsilon\to 0}\left(1-\frac{m\kappa}{m\kappa+m}\right)^{-m-1} {}_2\mathrm{F}_1\left(m+1, \frac{\beta}{\epsilon}; 2; \frac{\frac{-s\epsilon\xi\Omega}{m(1+\kappa)}}{1-\frac{m\kappa}{m\kappa+m}}\right) \\
&\overset{(b)}{=} \left(1-\frac{m\kappa}{m\kappa+m}\right)^{-m-1} {}_1\mathrm{F}_1\left(m+1, 2; \frac{\frac{-s\xi\Omega}{m(1+\kappa)}}{1-\frac{m\kappa}{m\kappa+m}}\right),
\end{aligned} \tag{69}$$

where (a) follows form using (56) and applying the reduction formulas [23, eq. (9.182.2)]

$$\mathrm{F}_2\left(\alpha, \beta, b, c, b; x, y\right) = (1-x)^{-\alpha} {}_2\mathrm{F}_1\left(\alpha, \beta; c; \frac{y}{1-x}\right), \tag{70}$$

and (b) follows from evaluating the limit according to $\lim_{\epsilon\to 0} {}_2\mathrm{F}_1\left(\alpha, \frac{b'}{\epsilon}; c'; \epsilon z\right) = {}_1\mathrm{F}_1\left(b'; \gamma; z\right)$. Substituting (69) into (6) yields the desired result after some simplifications. The Laplace transform of the aggregate interference under Nakagami-m fading, i.e., $\mathcal{L}^m_I$, specialises from $\mathcal{L}^{S\kappa\mu}_I$ when $m_I = \mu_I$. In this case, its is straightforward to show that the second summation in the RHS of (7) vanishes while the first summation reduces to $\mathcal{L}^m_I$.

E. Proof of C^m

Setting $m = \mu$ in (30) and resorting to [41, Th. 1], we have

$$\begin{aligned}
&\mathrm{F}_2\left(\mu+1, m, 1; \mu, 2; \frac{\mu\kappa}{\mu\kappa+m}, \frac{-\zeta\Omega}{\mu(1+\kappa)}\right) \\
&= \frac{(1+\kappa)}{\xi\Omega} {}_2\mathrm{F}_1\left(\mu, m; \mu; \frac{\mu\kappa}{\mu\kappa+m}\right) \\
&\quad - \frac{(1+\kappa) {}_2\mathrm{F}_1\left(\mu, m; \mu; \frac{\frac{\mu\kappa}{\mu\kappa+m}}{1+\frac{\xi\Omega}{\mu(1+\kappa)}}\right)}{\xi\Omega\left(1+\frac{\xi\Omega}{\mu(1+\kappa)}\right)^{\mu}} \\
&\overset{(b)}{=} \frac{(\kappa+1)^{m+1}}{\Omega\xi}\left(1-\left(1+\frac{\xi\Omega}{m}\right)^{-m}\right),
\end{aligned} \tag{71}$$

where (b) follows form applying ${}_2\mathrm{F}_1\left(a, b; b; z\right) = (1-z)^{-a}$. Substituting (71) into (30) yields the desired result after some manipulations.

F. Proof of $\mathcal{B}^{S\kappa\mu}(\lambda, \alpha)$

Using Craig's alternative expression for the Gaussian Q-function [26, eq. (9)], it is possible to reexpress (42) in terms of the MGF of the SINR as

$$\mathcal{B} = \frac{\beta_M}{\pi} \sum_{p=1}^{\tau_M} \int_0^{\pi/2} M_{\mathrm{SINR}}\left(\frac{a_p^2}{2\sin^2(\theta)}\right) d\theta. \tag{72}$$

Under shadowed κ-μ fading, substituting the SINR MGF by its expression in (6) and swapping the integration order gives

$$\begin{aligned}
&\mathcal{B}^{S\kappa\mu}(\lambda, \alpha) \\
&= \frac{\beta_M}{2} - \frac{A\beta_M\Gamma(\mu+1)}{2\pi B^{\mu+1}} \sum_{p=1}^{\tau_M} a_p^2 \int_0^{\infty} \\
&\quad \times \left(\int_0^{\pi/2} \frac{\Psi_1\left(\mu+1, m; 2, \mu; \frac{-a_p^2\xi\Omega}{2\sin^2(\theta)\mu(1+\kappa)}, \frac{\mu\kappa}{\mu\kappa+m}\right)}{\sin^2(\theta)} d\theta\right) \\
&\quad \times \mathcal{E}_r\left[\exp(-\xi r^{\alpha}\sigma^2)\mathcal{L}^{S\kappa\mu}_I\left(\xi r^{\alpha}\right)\right] d\xi,
\end{aligned} \tag{73}$$

Denote by Υ the inner integral in the RHS of (73) and let $t = \sin^2(\theta)$. Then after some manipulation one obtains

$$\Upsilon = \frac{1}{2}\int_0^1 \frac{\Psi_1\left(\mu+1, m; 2, \mu; \frac{-a_p^2\xi\Omega}{2t\mu(1+\kappa)}, \frac{\mu\kappa}{\mu\kappa+m}\right)}{t^{\frac{3}{2}}\sqrt{1-t}} dt. \tag{74}$$

To solve Υ we recall the single integral representation of the Humbert function $\Psi_1(a; b; c, c'; z, w)$, for $|w| < 1$, given in [34] as

$$\begin{aligned}
&\Psi_1\left(a, b; c, c'; w, z\right) \\
&\quad = \frac{\Gamma(c)}{\Gamma(b)\Gamma(c-b)} \int_0^1 t^{b-1}(1-t)^{c-b-1}(1-tw)^{-a} \\
&\qquad \times {}_1\mathrm{F}_1\left(a; c', \frac{z}{1-tw}\right) dt,
\end{aligned} \tag{75}$$

Substituting Ψ_1 by its integral representation in (74) and resorting to

$$\begin{aligned}
&\int_0^1 \frac{{}_1\mathrm{F}_1\left(a+1, b+1; -\frac{c}{x}\right)}{x^{3/2}\sqrt{1-x}} dx \\
&\quad = \sqrt{\frac{\pi}{c}} \frac{\Gamma(a+\frac{1}{2})\Gamma(b+1)}{\Gamma(1+a)\Gamma(b+\frac{1}{2})} {}_1\mathrm{F}_1\left(a+\frac{1}{2}, b+\frac{1}{2}; -c\right),
\end{aligned} \tag{76}$$

we obtain

$$\begin{aligned}
\Upsilon &= \frac{2\sqrt{2}\Gamma(\mu+\frac{1}{2})\sqrt{\frac{\mu(1+\kappa)}{\Omega}}}{\Gamma(\mu+1)\sqrt{\xi}} \\
&\quad \times \Psi_1\left(\mu+\frac{1}{2}, m; \frac{3}{2}, \mu; \frac{-a_p^2\xi\Omega}{2\mu(1+\kappa)}, \frac{\mu\kappa}{\mu\kappa+m}\right).
\end{aligned} \tag{77}$$

Substituting Υ by its expression in (73) yields the desired result after some simplifications.

G. Proof of $\mathcal{B}^{S\kappa\mu,\infty}(\alpha)$

Carrying out the change of variable $x = \Omega\xi$ in (47) and using [42, Ch. 5, eq. (2)], we have

$$ {}_2\mathrm{F}_1\left(-\frac{2}{\alpha}, m_I; 1-\frac{2}{\alpha}; -\frac{\Omega_I}{\Omega m_I}x\right) \underset{\frac{\Omega_I}{\Omega}\to 0}{\approx} 1+\frac{2\Omega_I}{\Omega(\alpha-2)}x, \quad (78) $$

Subsequently, the following integral arises from (48):

$$ \mathcal{J} = \int_0^\infty \frac{\Psi_1\left(\mu+\frac{1}{2}, m; \frac{3}{2}, \mu; \frac{-a_p^2 x}{2\mu(1+\kappa)}, \frac{\mu\kappa}{\mu\kappa+m}\right)}{\sqrt{x}\left(1+\frac{2\Omega_I}{\Omega(\alpha-2)}x\right)}dx. \quad (79) $$

To solve $\mathcal{J}$, we introduce the integral representation of the Humbert function Ψ_1 given by [34]

$$ \begin{aligned} &\Psi_1\left(a, b; c, c'; w, z\right) \\ &= \frac{\Gamma(c')}{\Gamma(a)} z^{\frac{1-c'}{2}} \int_0^\infty t^{a-(c'+1)/2} e^{-t} \\ &\quad \times \mathrm{I}_{c'-1}(2\sqrt{tz})\,{}_1\mathrm{F}_1\left(b; c, tw\right) dt, \quad \mathrm{Re}(a) > 0, \ |w| < 1. \end{aligned} \quad (80) $$

Then substituting (80) into $\mathcal{J}$ and swapping the integration order generate an integral of the form

$$ \begin{aligned} &\int_0^\infty \frac{\mathrm{I}_{\frac{1}{2}}\left(\sqrt{\frac{-2a_p^2 xt}{\mu(1+\kappa)}}\right)}{x^{3/4}\left(1+\frac{2\Omega_I}{\Omega(\alpha-2)}x\right)}dx \\ &\qquad = \sqrt{\pi}\left(\frac{-a_p^2 t}{2\mu(1+\kappa)}\right)^{-\frac{1}{4}}\left(1-e^{-\frac{\sqrt{\frac{a_p^2 t}{\mu(1+\kappa)}}}{\sqrt{\frac{\Omega_I}{\Omega(\alpha-2)}}}}\right). \end{aligned} \quad (81) $$

Let $\delta = \frac{\Omega(\alpha-2)}{\Omega_I}$, then resorting to the representation $e^z = \sqrt{\frac{z\pi}{2}}\left(\mathrm{I}_{\frac{1}{2}}(z) + \mathrm{I}_{-\frac{1}{2}}(z)\right)$ and using [23, eqs. (7.621.4) and (9.121.1)], we obtain $\mathcal{J}$, after several manipulations, as

$$ \begin{aligned} \mathcal{J} &= \sqrt{2\pi}\frac{\Gamma(\mu)\Gamma(\frac{3}{2})\sqrt{\mu(1+\kappa)}}{\Gamma(\mu+\frac{1}{2})a_p}\left(\frac{m}{\mu\kappa+m}\right)^{-m} \\ &\quad + \frac{\pi\delta^{\frac{1}{2}}}{\sqrt{2}}\Psi_1\left(\mu+\frac{1}{2}, m; \frac{3}{2}, \mu; \frac{a_p^2\delta}{4\mu(1+\kappa)}, \frac{\mu\kappa}{\mu\kappa+m}\right) \\ &\quad - \frac{\pi\Gamma(\mu)\sqrt{\mu(1+\kappa)}}{\sqrt{2}a_p\Gamma(\mu+\frac{1}{2})}\Psi_1\left(\mu, m; \frac{1}{2}, \mu; \frac{a_p^2\delta}{4\mu(1+\kappa)}, \frac{\mu\kappa}{\mu\kappa+m}\right) \end{aligned} \quad (82) $$

Tacking all these facts into consideration yields the desired result after some manipulations.

H. Proof of $\mathcal{B}^{m,\infty}(\alpha)$

From (46) and (78), the high SIR BEP under Nakagami-m fading involves an integral of the form

$$ \mathcal{K} = \int_0^\infty \frac{{}_1\mathrm{F}_1\left(m+\frac{1}{2}, \frac{3}{2}; \frac{-a_p^2\xi}{2m}\right)}{\sqrt{\xi}\left(1+\frac{2\Omega_I}{\Omega(\alpha-2)}\xi\right)}d\xi, \quad (83) $$

which can be solved using [23, eqs. (7.623.1) and (9.210.2)] after recognizing that ${}_1\mathrm{F}_1\left(m+\frac{1}{2}, \frac{3}{2}; \frac{-a_p^2\xi}{2m}\right) = e^{-\frac{a_p^2\xi}{2m}}\,{}_1\mathrm{F}_1\left(1-m, \frac{3}{2}; \frac{a_p^2\xi}{2m}\right)$. We then obtain

$$ \begin{aligned} \mathcal{K} &= -\frac{\pi\Gamma(m)\sqrt{m}}{\sqrt{2}a_p\Gamma(m+\frac{1}{2})}\left({}_1\mathrm{F}_1\left(m, \frac{1}{2}; \frac{a_p^2\Omega(\alpha-2)}{4m\Omega_I}\right)-1\right) \\ &\quad + \frac{\pi\,{}_1\mathrm{F}_1\left(m+\frac{1}{2}, \frac{3}{2}; \frac{a_p^2\Omega(\alpha-2)}{4m\Omega_I}\right)}{\sqrt{\frac{2\Omega_I}{\Omega(\alpha-2)}}}. \end{aligned} \quad (84) $$

Substituting the latter result in $\mathcal{B}^{m,\infty}(\alpha)$ and resorting to [23, eq. (9.210.2)] completes the proof.

REFERENCES

[1] J. G. Andrews, F. Baccelli, and R. K. Ganti, "A tractable approach to coverage and rate in cellular networks," *IEEE Trans. Commun.*, vol. 59, no. 11, pp. 3122–3134, Nov. 2011.

[2] H. S. Dhillon, R. K. Ganti, F. Baccelli, and J. G. Andrews, "Modeling and analysis of K-tier downlink heterogeneous cellular networks," *IEEE J. Sel. Areas Commun.*, vol. 30, no. 3, pp. 550–560, Apr. 2012.

[3] H. Elsawy, E. Hossain, and M. Haenggi, "Stochastic geometry for modeling, analysis, and design of multi-tier and cognitive cellular wireless networks: A survey," *IEEE Commun. Surveys Tuts.*, vol. 15, no. 3, pp. 996–1019, Jun. 2013.

[4] A. Guo and M. Haenggi, "Spatial stochastic models and metrics for the structure of base stations in cellular networks," *IEEE Trans. Wireless Commun.*, vol. 12, no. 11, pp. 5800–5812, Nov. 2013.

[5] M. Di Renzo and W. Lu, "The equivalent-in-distribution (EiD)-based approach: On the analysis of cellular networks using stochastic geometry," *IEEE Commun. Lett.*, vol. 18, no. 5, pp. 761–764, May 2014.

[6] Y. Lin, W. Bao, W. Yu, and B. Liang, "Optimizing user association and spectrum allocation in HetNets: A utility perspective," *IEEE J. Sel. Areas Commun.*, vol. 33, no. 6, pp. 1025–1039, Jun. 2015.

[7] M. Mirahsan, R. Schoenen, and H. Yanikomeroglu, "HetHetNets: Heterogeneous traffic distribution in heterogeneous wireless cellular networks," *IEEE J. Sel. Areas Commun.*, vol. 33, no. 10, pp. 2252–2265, Oct. 2015.

[8] A. Adhikary, H. S. Dhillon, and G. Caire, "Massive-MIMO meets HetNet: Interference coordination through spatial blanking," *IEEE J. Sel. Areas Commun.*, vol. 33, no. 6, pp. 1171–1186, Jun. 2015.

[9] L. H. Afify, H. ElSawy, T. Y. Al-Naffouri, and M.-S. Alouini, "A unified stochastic geometry model for MIMO cellular networks with retransmissions," *IEEE Wireless Commun.*, vol. 15, no. 12, pp. 8595–8609, Dec. 2016.

[10] H. ElSawy, A. Sultan-Salem, M.-S. Alouini, and M. Z. Win, "Modeling and analysis of cellular networks using stochastic geometry: A tutorial," *IEEE Commun. Surveys Tuts.*, vol. 19, no. 1, pp. 167–203, 1st Quart., 2017. [Online]. Available: https://arxiv.org/abs/1604.03689

[11] L. H. Afify, H. ElSawy, T. Y. Al-Naffouri, and M.-S. Alouini, "The influence of Gaussian signaling approximation on error performance in cellular networks," *IEEE Commun. Lett.*, vol. 19, no. 12, pp. 2202–2205, Dec. 2015.

[12] M. D. Yacoub, "The κ-μ distribution and the η-μ distribution," *IEEE Antennas Propag. Mag.*, vol. 49, no. 1, pp. 68–81, Feb. 2007.

[13] N. C. Beaulieu and X. Jiandong, "A novel fading model for channels with multiple dominant specular components," *IEEE Wireless Commun. Lett.*, vol. 4, no. 1, pp. 54–57, Feb. 2015.

[14] M. Mirahmadi, A. Al-Dweik, and A. Shami, "Interference modeling and performance evaluation of heterogeneous cellular networks," *IEEE Trans. Commun.*, vol. 62, no. 6, pp. 2132–2144, Jun. 2014.

[15] S. Rangan, T. S. Rappaport, and E. Erkip, "Millimeter-wave cellular wireless networks: Potentials and challenges," *Proc. IEEE*, vol. 102, no. 3, pp. 366–385, Mar. 2014.

[16] M. Di Renzo and P. Guan, "Stochastic geometry modeling of coverage and rate of cellular networks using the Gil–Pelaez inversion theorem," *IEEE Commun. Lett.*, vol. 18, no. 9, pp. 1575–1578, Sep. 2014.

[17] M. Di Renzo, A. Guidotti, and G. E. Corazza, "Average rate of downlink heterogeneous cellular networks over generalized fading channels: A stochastic geometry approach," *IEEE Trans. Commun.*, vol. 61, no. 7, pp. 3050–3071, Jul. 2013.
[18] A. Al-Hourani and S. Kandeepan, "On modeling coverage and rate of random cellular networks under generic channel fading." [Online]. Available: https://arxiv.org/abs/1605.08381
[19] A. AlAmmouri, H. ElSawy, A. Sultan-Salem, M. Di Renzo, and M.-S. Alouini, "Modeling cellular networks in fading environments with dominant specular components," in *Proc. IEEE Int. Conf. Commun. (ICC)*, May 2016, pp. 1–7.
[20] J. F. Paris, "Statistical characterization of κ-μ shadowed fading," *IEEE Trans. Veh. Technol.*, vol. 63, no. 2, pp. 518–526, Feb. 2014.
[21] S. Parthasarathy and R. K. Ganti, "SIR distribution in downlink Poisson point cellular network with κ-μ shadowed fading," *IEEE Wireless Commun. Lett.*, vol. 6, no. 1, pp. 10–13, Feb. 2017.
[22] Y. J. Chun, S. L. Cotton, H. S. Dhillon, F. J. Lopez-Martinez, J. F. Paris, and S. K. Yoo, "A comprehensive analysis of 5G heterogeneous cellular systems operating over κ-μ shadowed fading channels," *CoRR*, Oct. 2016. [Online]. Available: https://arxiv.org/abs/1609.09696
[23] I. S. Gradshteyn and I. M. Ryzhik, *Table of Integrals, Series, and Products*, 5th ed. New York, NY, USA: Academic, 1994.
[24] S. L. Cotton, "Human body shadowing in cellular device-to-device communications: Channel modeling using the shadowed κ-μ fading model," *IEEE J. Sel. Areas Commun.*, vol. 33, no. 1, pp. 111–119, Jan. 2015.
[25] S. L. Cotton, "A statistical model for shadowed body-centric communications channels: Theory and validation," *IEEE Trans. Antennas Propag.*, vol. 62, no. 3, pp. 1416–1424, Mar. 2014.
[26] M. K. Simon and M.-S. Alouini, *Digital Communication Over Fading Channels*, vol. 95. Hoboken, NJ, USA: Wiley, 2005.
[27] F. Baccelli and B. Blaszczyszyn, *Stochastic Geometry and Wireless Networks, Part I: Theory*. Dordrecht, The Netherlands: Now Publishers, 2009.
[28] S. Singh, M. N. Kulkarni, A. Ghosh, and J. G. Andrews, "Tractable model for rate in self-backhauled millimeter wave cellular networks," *IEEE J. Sel. Areas Commun.*, vol. 33, no. 10, pp. 2196–2211, Oct. 2015.
[29] X. Zhang and J. G. Andrews, "Downlink cellular network analysis with multi-slope path loss models," *IEEE Trans. Commun.*, vol. 63, no. 5, pp. 1881–1894, May 2015.
[30] J. Gil-Pelaez, "Note on the inversion theorem," *Biometrika*, vol. 38, nos. 3–4, pp. 481–482, Dec. 1951.
[31] K. A. Hamdi, "Capacity of MRC on correlated Rician fading channels," *IEEE Trans. Commun.*, vol. 56, no. 5, pp. 708–711, May 2008.
[32] M. Di Renzo, F. Graziosi, and F. Santucci, "A unified framework for performance analysis of CSI-assisted cooperative communications over fading channels," *IEEE Trans. Commun.*, vol. 57, no. 9, pp. 2551–2557, Sep. 2009.
[33] V. A. Thomas, S. Kumar, S. Kalyani, M. El-Hajjar, K. Giridhar, and L. Hanzo, "Error vector magnitude analysis of fading SIMO channels relying on MRC reception," *IEEE Trans. Commun.*, vol. 64, no. 4, pp. 1786–1797, Apr. 2016.
[34] A. Yu Brychkova and N. Saad, "On some formulas for the Appell function $F_2(a, b, b'; c, c'; w; z)$," *Integral Transforms Special Funct.*, vol. 25, no. 2, pp. 111–123, 2014.
[35] L. Moreno-Pozas, F. J. Lopez-Martinez, J. F. Paris, and E. Martos-Naya, "The κ-μ shadowed fading model: Unifying the κ-μ and η-μ distributions," *IEEE Trans. Veh. Technol.*, vol. 65, no. 12, pp. 9630–9641, Dec. 2016.
[36] J. Abate and W. Whitt, "Numerical inversion of Laplace transforms of probability distributions," *ORSA J. Comput.*, vol. 7, no. 1, pp. 36–43, 1995.
[37] J. G. Proakis, *Digital Communications*, 4th ed. Singapore: McGraw-Hill, 2001.
[38] J. Ilow and D. Hatzinakos, "Analytic alpha-stable noise modeling in a Poisson field of interferers or scatterers," *IEEE Trans. Signal Process.*, vol. 46, no. 6, pp. 1601–1611, Jun. 1998.
[39] P. C. Pinto and M. Z. Win, "Communication in a Poisson field of interferers—Part I: Interference distribution and error probability," *IEEE Trans. Wireless Commun.*, vol. 9, no. 7, pp. 2176–2186, Jul. 2010.
[40] L. Rubio, J. Reig, and N. Cardona, "Evaluation of Nakagami fading behaviour based on measurements in urban scenarios," *AEU-Int. J. Electron. Commun.*, vol. 61, no. 2, pp. 135–138, Feb. 2007.
[41] S. B. Opps, N. Saad, and H. M. Srivastava, "Some reduction and transformation formulas for the Appell hypergeometric function F_2," *J. Math. Anal. Appl.*, vol. 302, no. 1, pp. 180–195, Feb. 2005.
[42] A. Erdelyi, W. Magnus, F. Oberhettinger, and F. G. Tricomi, *Higher Transcendental Functions*, vol. 1. New York, NY, USA: McGraw-Hill, 1953.

Imène Trigui (S'10–M'15) received the B.Eng. degree (Hons.) in signals and systems from the Tunisia's Communications School (Sup'Com) in 2006, and the M.Sc. and Ph.D. degrees (Hons.) from the National Institute of Scientific Research (INRS-EMT), University of Quebec, Montreal, QC, Canada, in 2010 and 2015, respectively. She is currently a Post-Doctoral Research Fellow with the Department of Electrical Engineering, Toronto University, Toronto, ON, Canada. Her research interests are in wireless communications and signal processing.

In recognition of her academic, research, and scholarly achievements, she has been a recipient of several major awards, including the Natural Sciences and Engineering Research Council of Canada Post-Doctoral Fellowship from 2016 to 2018 and the top-tier Alexander-Graham-Bell Canada Graduate Scholarship from the National Sciences and Engineering Research Council from 2012 to 2014. She had to decline other Ph.D. and post-doctoral scholarships offered over the same period from the Fonds de recherche du Québec—Nature et technologies. She was a recipient of an undergraduate student fellowship from the Tunisian Ministry of Communications. She also received a Best Paper Award at the IEEE VTC'2010-Fall. She serves regularly as a reviewer for many top international journals and conferences in her field.

Sofiène Affes (S'95–SM'05) received the Diplôme d'Ingénieur in telecommunications and the Ph.D. degree (Hons.) in signal processing from the École Nationale Supérieure des Télécommunications, Paris, France, in 1992 and 1995, respectively. He was a Research Associate with INRS, Montreal, QC, Canada, until 1997, an Assistant Professor until 2000, and an Associate Professor until 2009. He is a currently a Full Professor and the Director of PERWADE, a unique U.S. $4 million research training program on wireless in Canada involving 27 faculty from 8 universities and 10 industrial partners. He has been twice a recipient of a Discovery Accelerator Supplement Award from NSERC, from 2008 to 2011 and from 2013 to 2016. In 2008 and 2015, he received the IEEE VTC Chair Recognition Award from the IEEE VTS and the IEEE ICUWB Chair Recognition Certificate from the IEEE MTT-S for exemplary contributions to the success of the IEEE VTC and the IEEE ICUWB, respectively. In 2006 and 2015, he served as a General Co-Chair of the IEEE VTC'2006-Fall and the IEEE ICUWB'2015, respectively, both held in Montreal, QC, Canada. From 2003 to 2013, he was a Canada Research Chair in wireless communications. He will act as a General Chair of the IEEE PIMRC'2017 to be held in Montreal, QC, Canada. He was an Associate Editor of the IEEE TRANSACTIONS ON WIRELESS COMMUNICATIONS from 2007 to 2013 and the IEEE TRANSACTIONS ON SIGNAL PROCESSING from 2010 to 2014. He is currently an Associate Editor of the IEEE TRANSACTIONS ON COMMUNICATIONS and the *Wireless Communications and Mobile Computing* journal (Wiley).

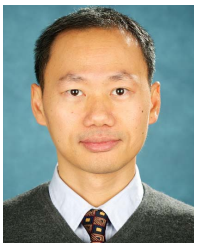

Ben Liang (S'94–M'01–SM'06) received the B.Sc. (valedictorian) and M.Sc. degrees in electrical engineering from Polytechnic University, Brooklyn, New York, in 1997, and the Ph.D. degree in electrical engineering with a minor in computer science from Cornell University, Ithaca, New York, in 2001. In 2001 and 2002, he was a Visiting Lecturer and a Post-Doctoral Research Associate with Cornell University. He joined the Department of Electrical and Computer Engineering, University of Toronto, in 2002, where he is currently a Professor. His current research interests are in networked systems and mobile communications. He is a member of ACM and Tau Beta Pi. He has been serving as an Editor of the IEEE TRANSACTIONS ON COMMUNICATIONS since 2014, and he was an Editor of the IEEE TRANSACTIONS ON WIRELESS COMMUNICATIONS from 2008 to 2013 and an Associate Editor of the *Security and Communication Networks* journal (Wiley) from 2007 to 2016. He regularly serves on the organizational and technical committees of a number of conferences.